A Statistical Model for Liquid Propellant Rocket Engine Dry Weight

by

Sarvesh Janarthanan

A thesis submitted to the Graduate Faculty of
Auburn University
in partial fulfillment of the
requirements for the Degree of
Master of Science

Auburn, Alabama
December 14, 2019

Keywords: Liquid Propellant Rocket Engine, Statistical Analysis, Similitude, Scaling, Regression

Approved by

Roy Hartfield, Chair, Walt and Virginia Waltosz Professor of Aerospace Engineering

Mark Carpenter, Professor, Department of Mathematics and Statistics

Joseph Majdalani, Francis Chair, Department of Aerospace Engineering

Abstract

The principle of similitude is applied to liquid propellant rocket engine dry weight using a statistical approach to produce a conceptual design level model. The argument of similitude is extended from basic physics scaling to a statistically reliable prediction tool. Dry weight of the engine is found to be well correlated with thrust for a wide range of designs, propellant combinations and cycles. These statistically defensible results can be used for trade studies, reverse engineering, explaining the relationships between engineering principles and performance, and sizing in conceptual design. This thesis is an extension of a similar attempt [1] which addresses the development of the model for liquid propellant rocket engine dry mass using a range of mathematical/statistical approaches and presents the working model with associated results.

Acknowledgments

The author would like to thank his family, especially parents, for their years of unwavering support and encouragement throughout his academic endeavors. The author is thankful to Dr. Roy Hartfield for taking a chance on him and giving an opportunity to work on a unique research project and for his continued support, guidance and encouragement throughout the process. Author would like to thank Dr. Mark Carpenter and Jordan Eckert for their help with data modelling and for their continual support and assistance throughout the duration of the project. Author would like to thank Dr. Joseph Majdalani for agreeing to be on his thesis committee and also for his continued support for the project. Author is incredibly lucky to have their support and support of many others along the way.

Table of Contents

List of Tables

List of Figures

List of Abbreviations

MCC – Main Combustion Chamber

GG – Gas Generator

MFV – Main Fuel Valve

MOV – Main Oxidizer Valve

GGFV – Gas Generator Fuel Valve

GGOV – Gas Generator Oxidizer Valve

OTBV – Oxidizer Turbine Bypass Valve

CCV – Coolant-Control Valve

PBOV – Preburner Oxidizer Valve

MAE – Mean Absolute Error

MAPE – Mean Absolute Percentage Error.

RMSE – Root Mean Square Error

CHAPTER 1

INTRODUCTION

1.1 Overview

Similitude is a foundational geometrically derived principle which drives mass to performance efficiency of a wide range of systems. Similitude explains why scaled up engines are more efficient while scaled down engines are less efficient, why large aircraft are dramatically more stable in air disturbances than small aircraft, why the chamber pressure in solid propellant rocket motor is nearly constant with length scale and many other conceptual rules. Similitude for rocket engines has been explored by way of physics arguments by Barrere et al.[2]

While the concept of similitude applies in a simple, intuitive way to solid propellant rocket motors, for liquid propellant rocket engines the same concept is less intuitive because of the lack of a direct connection between the length scale of the thrust chamber and the turbo-pumps or other pressurization hardware. Nevertheless, some fundamental physical scaling is fundamental and can be extracted. For example, in combustion instability studies, it can be shown that in some cases, the maximum change in pressure normalized by the average pressure scales with length scale.

From a design perspective, Barrere et al. [2] showed that combustor pressure ratios and characteristic velocities can be scaled using a characteristic length n_d as depicted in Figure 1. The injection diameters can also be scaled using characteristic lengths and velocities. A relationship is provided in Barrere for throat diameter scaling with length scale and the cooling systems size scales linearly with length scale.

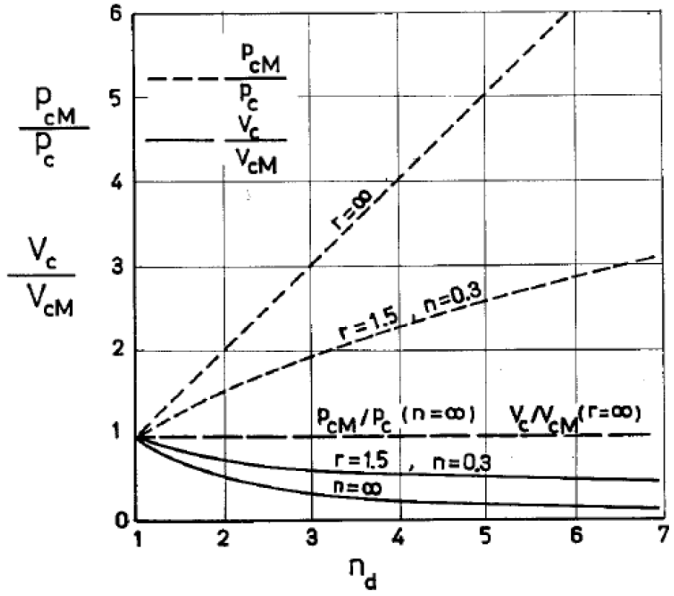

Figure 1: The effect of Scale on pressures and velocities, for various assumptions regarding the characteristic time [Barrere et. al. [2]]

While useful as design rules, these similitude arguments for liquid propellant rocket engines have not been as extensively explored for large scale design as the similitude arguments applied to solid propellant rocket motors, perhaps because the confluence of the similitude arguments for liquid propellant rocket engines is not as transparent to the conceptual design process for liquid propellant rocket engines. This work seeks to extend the classical arguments for similitude to the conceptual design arena where similitude can be used for preliminary design mass calculation which can be reduced to primarily a function of required thrust. This same concept, if successful might be useful in efforts to reverse engineer existing liquid rocket systems.

Moreover, in the development of new technology for liquid propellant rocket engines, a topological map of performance at different technology levels could be useful in making decisions about power cycles, new/legacy manufacturing techniques, companion mechanical design and costs. Some factors that influence the topology include specific impulse, basic propellant properties, scale of the engine, nozzle expansion ratio, cycle and engine technology level to include materials, manufacturing methods, design of components and chamber pressure. The following section will provide a brief explanation of some fundamental parameters of the engine used in this work.

1.2 Thrust

Thrust (T) is the force produced by a rocket propulsion system acting upon a vehicle. In simple words, it is the reaction experienced by a nozzle structure due to the ejection of matter at high velocity. In rocket propulsion relatively small masses are involved which are carried within the vehicle and ejected at high velocities [3]. In a liquid rocket, stored fuel and stored oxidizer are pumped into a combustion chamber where they are mixed and burned. The combustion produces great amounts of exhaust gas at high temperature and pressure. The hot exhaust is passed through a nozzle which accelerates the flow. Thrust is produced according to Euler's formulation of Newton's second law of motion known broadly as the momentum equation of fluid dynamics. A schematic of liquid rocket engine is shown in Figure 2.

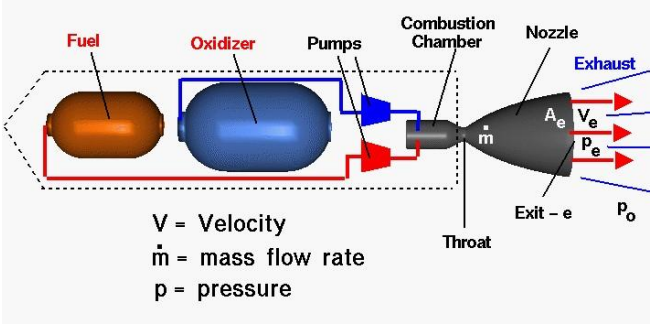

Figure 2: Liquid Rocket Engine Schematic [4].

The amount of thrust produced by a given rocket depends on the mass flow rate through the engine, the exit velocity of the exhaust, and the pressure at the exit. The smallest cross-section area of the nozzle is called the throat of the nozzle. Specific impulse is a broadly used a measure of efficiency [4].

1.3 Specific impulse

Specific impulse (I_{sp}) is a measure of how effectively a rocket uses propellant to produce thrust. By definition, it is the total impulse (or change in momentum) delivered per unit of propellant consumed [5] and is dimensionally equivalent to the generated thrust divided by the propellant mass flow rate or weight flow rate [6]. If weight is used as the unit of propellant, then specific impulse has units of time (seconds). The higher the specific impulse, the less propellant is needed to produce a given thrust for a given time. In this regard a propellant is more efficient the greater its specific impulse. Figure 3 shows a plot of the specific impulse for several types of rockets. As noticed, chemical rockets have a limited range of specific impulse.

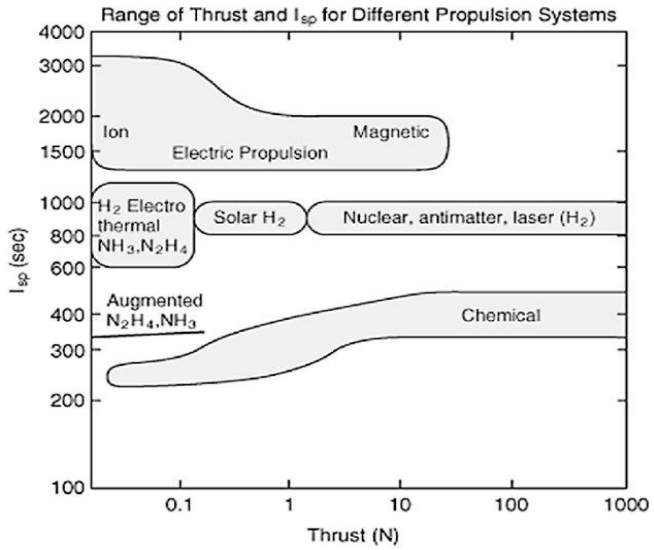

Figure 3. Specific impulse compared with thrust for several propulsion systems [7].

1.4 Thrust to weight ratio

The ratio of thrust produced by a rocket engine to its dry weight is by definition thrust to weight ratio. Thrust to weight ratio is a dimensionless quantity which can be used as a figure of merit for comparing the performance of rocket. It can also be an indicator of the rocket's acceleration expressed in multiples of gravitational acceleration [3]. The thrust to weight ratio for a rocket varies continually during operation due to progressive consumption of propellant. For a constant thrust the maximum ratio is achieved just before the propellant is fully consumed. Each rocket has a characteristic thrust to weight curve or acceleration curve. A high thrust to weight ratio leads to high speed in the lower atmosphere which increases aerodynamic pressure and heating. Lower thrust to weight ratio means the rocket will take longer to reach orbital speed which leads to high gravity losses. For a takeoff from the surface of earth using thrust and no aerodynamic lift, the thrust to weight ratio for the whole vehicle is generally slightly more than one for many orbital launchers [3]. Figure 4 shows plot of thrust to weight ratio as a measure of gravitational acceleration based on different propellant technologies.

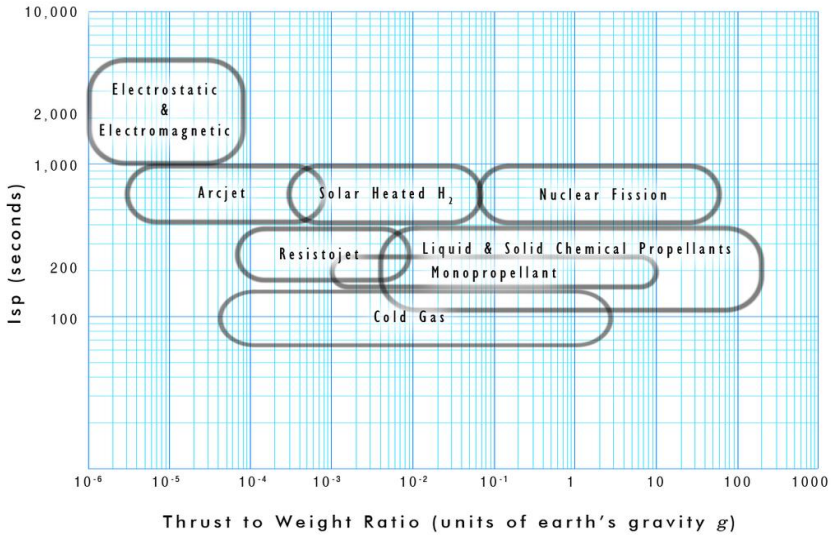

Figure 4: Thrust weight ratio vs Specific impulse for different propellant technologies [3].

1.5 Engine power cycle

Unlike solid rocket motors, the propellants in a liquid rocket engine are not burned where they are stored. A propellant transport mechanism from tanks to combustion chamber is equipped preferably with pressure increase. Methods of moving a propellant are generally classified into four main categories: pressure fed, turbopump gas generator, turbopump staged combustion and turbopump expander cycle. The selection of a cycle depends on application or mission requirements as one cycle is not universally applicable

1.5.1 Pressure fed cycle

The Pressurized gas fed cycle is the simplest cycle for rocket propulsion as it does not have pumps or turbines. It relies on tank pressure to feed the propellants into the combustion chamber. Performance is limited due to the size of the pressurant tank [8]. Also, relatively low chamber pressure is used because higher pressure makes the tanks too heavy. The cycle is reliable and has good throttleability. Depending on the type of propellant used the pump fed system can have one or more storage tanks. Astris, kestrel and AJ-10 are some of the engines that use pressure fed cycle.

1.5.2 Gas generator cycle

The gas generator cycle is a power cycle of a (usually) bipropellant rocket engine. It is also called open cycle as it taps off a small amount of fuel and oxidizer from the main flow to feed a burner called the gas generator. The hot gas from this generator passes through a turbine to generate power for the pumps that send propellants to the combustion chamber. The hot gas is then either dumped overboard or sent into the main nozzle downstream. The amount of thrust produced can be controlled by controlling the flow of propellants into the combustion chamber. The propellants are commonly burned at a less than optimal mixture ratio to keep the temperature low for the turbine blades. Most rocket engines in this cycle use regenerative cooling to cool the nozzle

and combustion chamber, increasing efficiency and allowing higher engine temperature [9]. Figure 6 shows the schematics of a gas generator cycle. F-1, J-2, Merlin, RD-108, RS-27, Viking are some of the engines that use gas generator cycle.

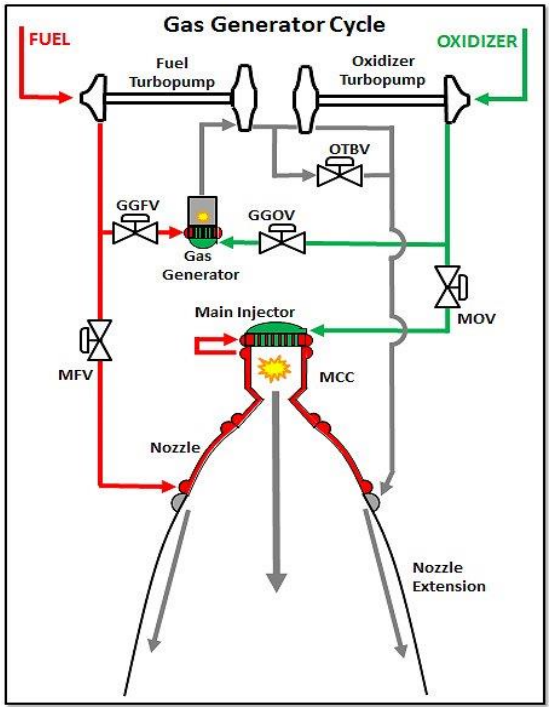

Figure 6. Schematic of a Gas Generator Cycle Engine [10].

1.5.3 Staged combustion cycle

The staged combustion cycle is a power cycle of a bipropellant rocket engine. It is also called closed cycle. The propellants are burned in stages, a preburner burns tapped off propellant producing an oxidizer or fuel rich hot gas mixture that is mostly unburned vaporized propellant. This hot gas is then injected into the combustion chamber after passing through the turbine. Figure 6 shows a simple schematic of a staged combustion cycle engine. All of the propellants are burned at an optimal mixture ratio in the combustion chamber and hence can be used for high power application. Higher chamber pressure generally leads to a smaller and lighter engine to produce the same amount of thrust. RD-180, SSME, AJ-26 are some of the engines that use staged combustion cycle.

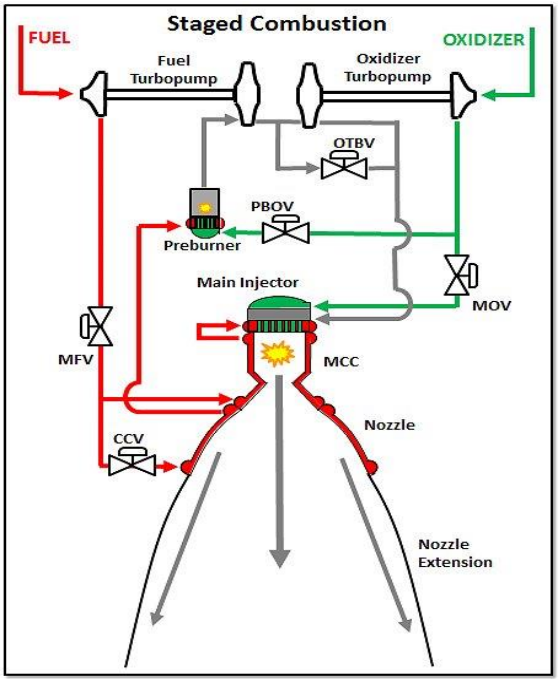

Figure 7. Schematic of a Staged Combustion Cycle Engine [10].

1.5.4 Expander cycle

The expander cycle is a power cycle of a bipropellant rocket engine. The cryogenic fuel is used to cool the combustion chamber aiding in phase change of the fuel which is then passed through the turbine before being injected into the combustion chamber to be burned with oxidizer. As in staged combustion there is no preburner and all of the propellants are burned at an optimal mixture ratio. Figure 8 shows a typical schematic of closed expander cycle. RL-10 and its variants use expander cycle.

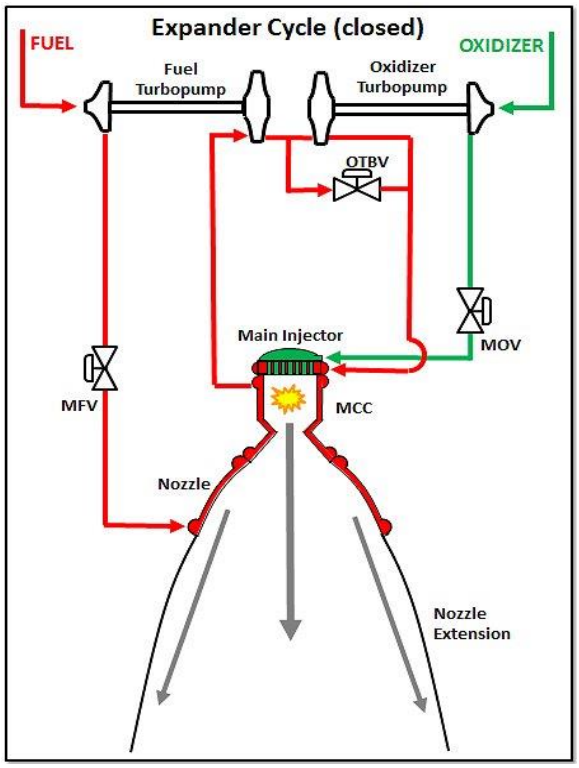

Figure 8. Schematic of an Expander cycle Engine [closed] [10].

CHAPTER 2

DATA DESCRIPTION

2.1 Overview

The full data set is included in Appendix A [11-47]. The data consist of qualitative variables (engine name and engine cycle) and quantitative variables related to performance (thrust, specific impulse, engine dry weight, thrust to weight ratio) from 211 liquid rocket engines. Table 1, below, summarizes the various engine types in the dataset, with respect to cycle and ISP level. There is only one count in electric pump fed as it is a relatively new type with low power application. Clearly, gas generator and staged combustion engines are the most common with expander cycle and pressure fed engines following behind. Table 2 contains summary statistics of the various performance variables in the data set.

Table 1: Frequencies of Engine types based on cycle and isp level

Cycle	**Count**	**Isp level**
Electric Pump Fed	1	343
Expander	18	335-470
Gas Generator	119	246-476
Pressure Fed	14	263-324
Staged Combustion	59	237-485

Table 2: Summary Statistics of Performance Variables

Variable	N	Mean	Std. Dev.	Min	Max
Thrust	211	1021.5	1856.513	5.3	17633
Dry weight	211	1160.4	1819.612	21.8	11703
TWR	211	77.219	45.11281	4.751	415.705
ISP	211	351.2	62.47185	237	485

2.2 Data Characterization

A range of variables traditionally considered to be of first order importance to rocket engine design are examined for variability in the data set. Clearly the data considered contain a range of engines scattered through the traditional design space.

2.2.1 Boxplot

Boxplot diagram is a graphical method typically depicted by quartiles and inter quartiles that helps in defining the upper and lower limit of data. Boxplot is also known as box and whisker's plot. It is a standardized way of displaying the distribution of data based on a five-number summary. The top and bottom lines of the rectangle are 3rd and 1st quartiles (Q3 and Q1), respectively. The length of the rectangle from top to bottom is the interquartile range (IQR). A line inside the box shows the median, which is not necessarily central. The top whisker (upper inner fence) denotes the maximum value or 3rd quartile plus 1.5 times the interquartile range (Q3+1.5*IQR). The bottom whisker (lower inner fence) denotes the minimum value or 1st quartile minus 1.5 times the interquartile range (Q1-1.5*IQR). The data points lying outside this inner

whisker are called mild outliers. Values outside the range [(Q1-3*IQR), (Q3+3*IQR)] or outer fences are known as extreme outliers. Boxplot can also tell us if our data is symmetrical, how tightly the data is grouped and if the data is skewed [48-50]. Figure 9 shows the boxplot of principle design variables from the dataset.

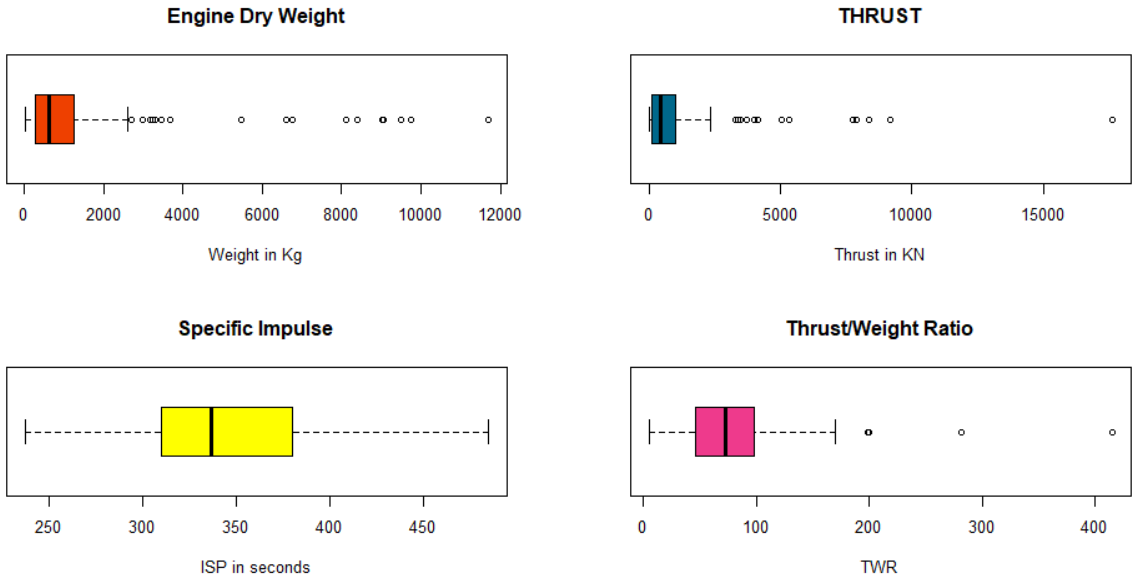

Figure 9: Boxplot of data topology based on principle design variables

We can see that the data for engine dry weight, thrust and thrust weight ratio is skewed to the right. Data is more centrally distributed for specific impulse. For engine dry weight, thrust and specific impulse the data to the right of median is more dispersed. Thrust to weight ratio has a centrally located median line which indicates an equally dispersed data on either side of the median line. Engine dry weight, thrust and thrust to weight ratio has few outliers beyond the upper fence/maximum line which is because the majority of the data is distributed towards the left extreme. Specific impulse has no outliers; hence a central and even dispersion of data is observed. This dispersion of data is visualized in Fig10 through histograms.

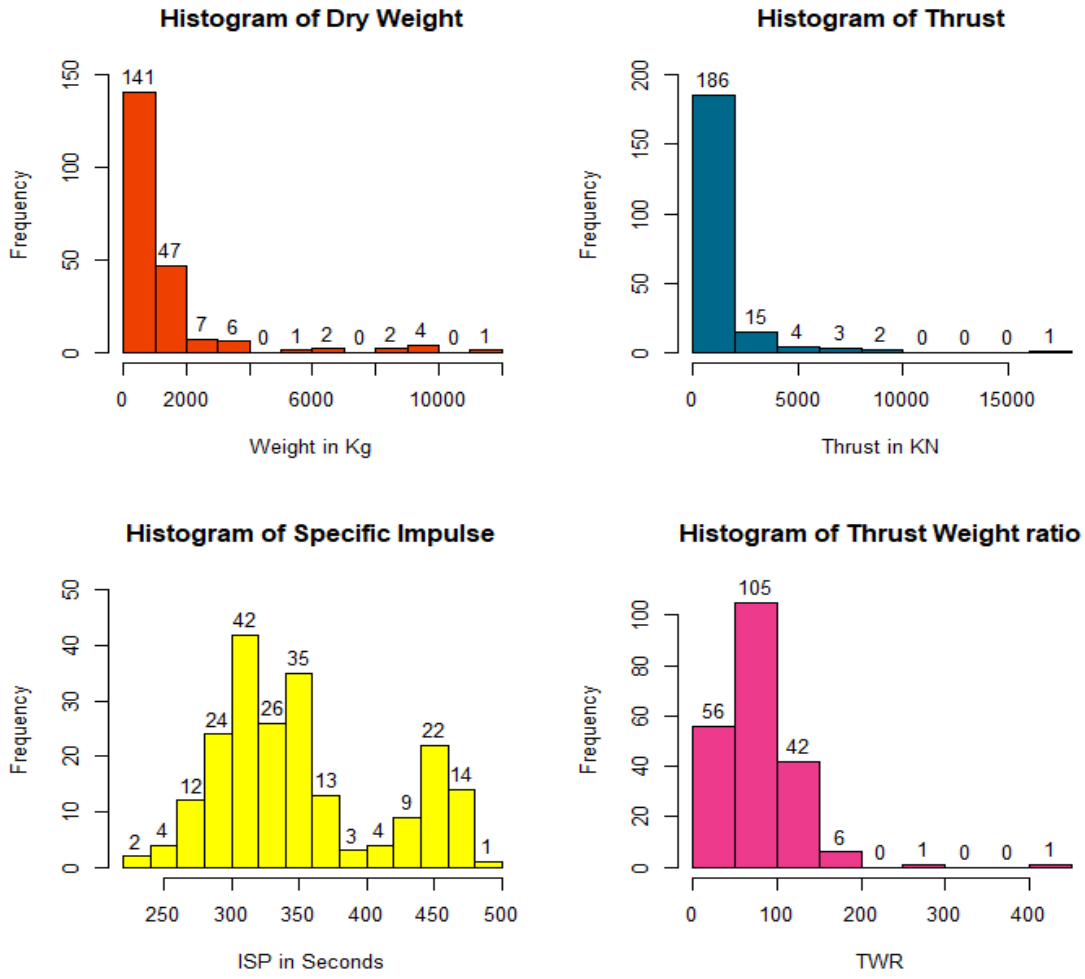

Figure 10: Histogram showing data dispersion of key design variables

Histogram confirms our inference of boxplot indication that engine dry weight, thrust and thrust to weight ratio are skewed to the right. We can see the number of data points indicated above each bar confirming that most of the data is concentrated within a certain range on the left of the graph. Specific impulse has almost centrally distributed bars which indicates dispersion of most of the data points around the center confirming boxplot inference. The statistical summary of boxplot for each design variable is summarized in table 3.

Table 3: Statistical summary of boxplot

Variable	N	Min. (Q1-1.5*IQR)	Q1	Median	Q3	Max. (Q3+1.5*IQR)	Outliers
Engine dry weight	211	-1179	274.5	643	1243.5	2697	19
Thrust	211	-1260.5	99.1	467	1005.5	2365.1	15
Specific impulse	211	205	310	337	380	485	0
Thrust weight ratio	211	-30.54	46.473	72.219	97.815	174.828	4

All the variables have 211 data points without any missing values. Engine dry weight has a lower inner fence of -1179 and upper inner fence of 2697. There are 19 data points beyond this upper inner fence and hence they are treated as outliers. Thrust has a lower inner fence of -1260.5 and upper inner fence of 2365.1. The 15 data points beyond the range of inner fences are treated as outliers. Specific impulse has a lower inner fence of 205 and upper inner fence of 485 which is equal to the maximum value of specific impulse from the dataset. There are zero outliers which is confirmed by the boxplot and histogram data dispersion. Thrust weight ratio has a lower inner fence of -30.54 and upper inner fence of 174.828 with 4 data points beyond this range. The number of outliers can be reduced by assuming that the values within the range of outer fences have no effect on the data during analysis. The number of outliers gets reduced to 10 in engine dry weight, 12 in thrust and 2 in thrust weight ratio. Further details about the effect of remaining outliers can be found from detailed analysis in next chapter. Also, next chapter explores a range of critical

variable combinations through data visualization and a regression model is built for the combinations to explain their correlation through statistics.

CHAPTER 3

DATA ANALYSIS

3.1. Overview

Data analysis is the process of systematically applying statistical or logical techniques to inspect, cleanse, describe, illustrate and model the data with goal of discovering useful information. To achieve a similitude-based approach at a system level, the range of data was collected for liquid rocket systems from around the world, systems of a variety of cycles, propellant combinations, manufacturing approaches and designers. This data was collected from a range of sources including Sutton's [11].

Data of engine performance and dimensional parameters were collected from various sources for more than 600 different liquid rocket engines. Since not every information about every single engine is available in the free web and also based on the necessary performance parameters the collected data was cleansed and condensed to about 211 engines. These include some of the famous engines like F-1, RD-180, RL-10 etc. The dataset consists of a mix of liquid propellant rocket engines from various countries like United States, Russia, United Kingdom, Germany, France, China, India, etc. Also, the engines have range of manufacturers from government organizations like NASA, ESA, ISRO to contractors like Aerojet Rocketdyne, Pratt & Whitney and private developers like SpaceX, Blue Origin etc.

All these organizations have their own propellant combinations, manufacturing approaches and designers, despite the physics being the same this difference in approach in building a fully functional rocket engine is bound to have some effects on the performance of the engine if we compare two engines of same thermodynamic cycle for a similar application. The engine in the dataset have a cocktail of applications ranging from being the main engine of the core stage to

being used in the final stage. The application of these engines greatly determines their performance characteristics. For example, an engine like F-1 which is used as the main engine in Saturn V produces high thrust and weighs heavier because it propels a heavy launch vehicle from the grasp of earth's gravity into space. An engine like CE-20 is used in the third stage of a GSLV MK III for in-space propulsion purposes has a low thrust value and low engine weight because of its place of application. Both the engines use the same gas generator cycle, since the place of application is different there is the extremities in the performance of these engines. These extremities in data could have some effect in our analysis. Previous chapter provided a preliminary understanding of the data through boxplots and histograms where we found some outliers which can be explained based on the previous example. To fully understand our data and obtain a statistically defensible relationship between performance variables these 211 data points are statistically explored further through data visualization and a regression model. A range of critical design variable combinations is explored, and a thrust weight comparison is considered for the purpose of demonstrating success.

3.2 Data Topology by Cycle

The summarized engine parameters are classified based on power cycle as described in chapter 1. Power cycle serves as an excellent factor for subgrouping the data, providing a better perspective into the dataset. Figure 11-12 shows the data spread based on cycle. Data is split into groups based on which operating cycle each engine uses and a boxplot for cycle is represented to visualize the data spread. We can see most of the engines from the dataset either use gas generator cycle or staged combustion cycle. Pressure fed and expander cycle have very few engines and there is only one data point in electric pump fed engines since it is a relatively newer concept. It will be unreliable to model each cycle individually as the number data points for each cycle is not comparable. Better results can be obtained by using a multiple regression approach for our analysis based on cycle.

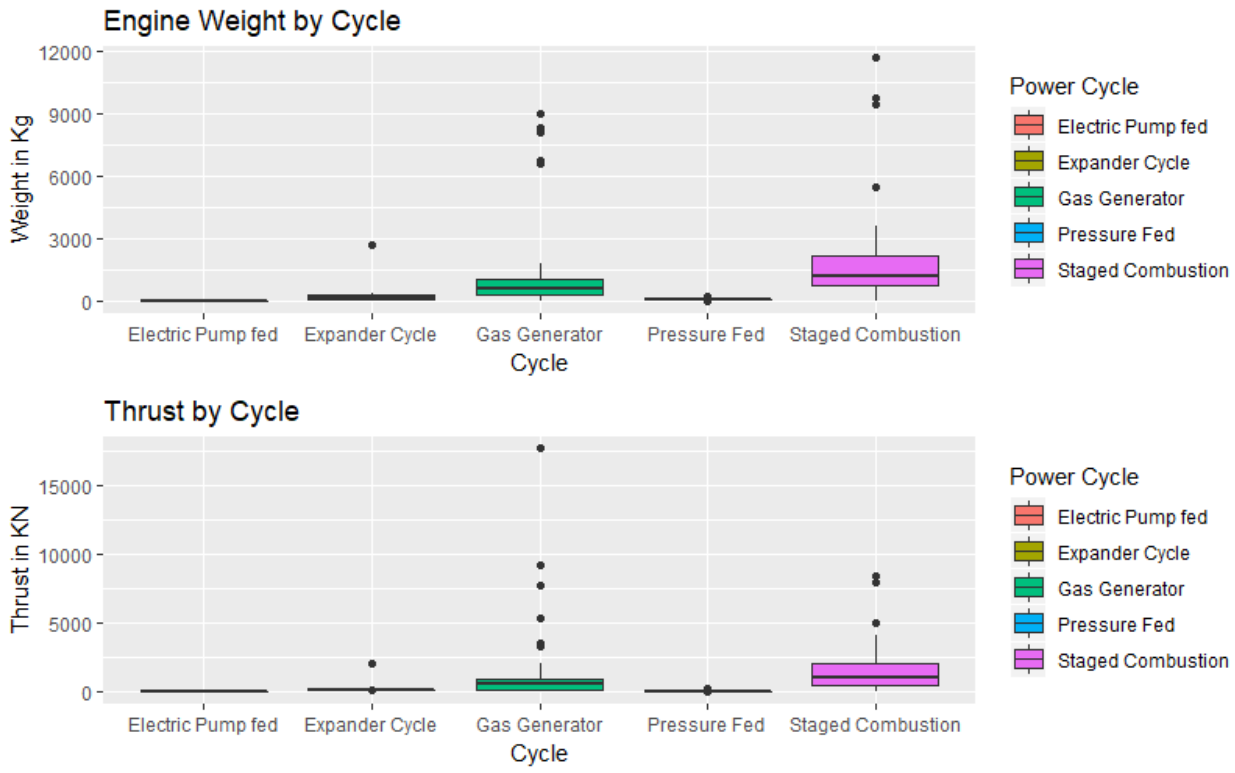

Figure 11: Engine dry weight and thrust based on cycle

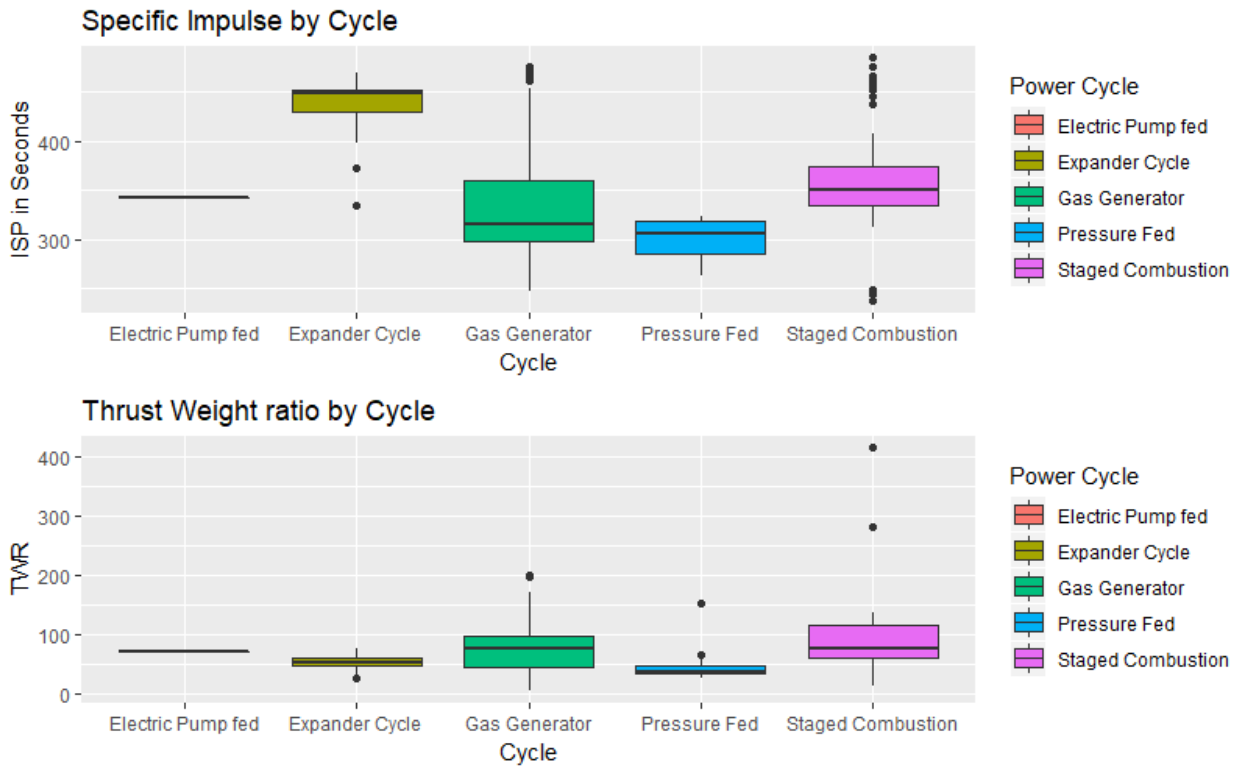

Figure 12: Specific impulse and thrust weight ratio based on cycle.

3.3 Weight - Thrust Analysis

As mentioned previously, engine dry weight-thrust combination is the main focus of our analysis. Figure 13 shows a scatter plot of engine dry weight against thrust. On a normal plot we cannot clearly say there is a linear relationship between the two variables. But from figure 14 we can see how the engine dry weight values are linearly distributed as a function of thrust on a log-log scale. This gives further motivation to continue with this analysis.

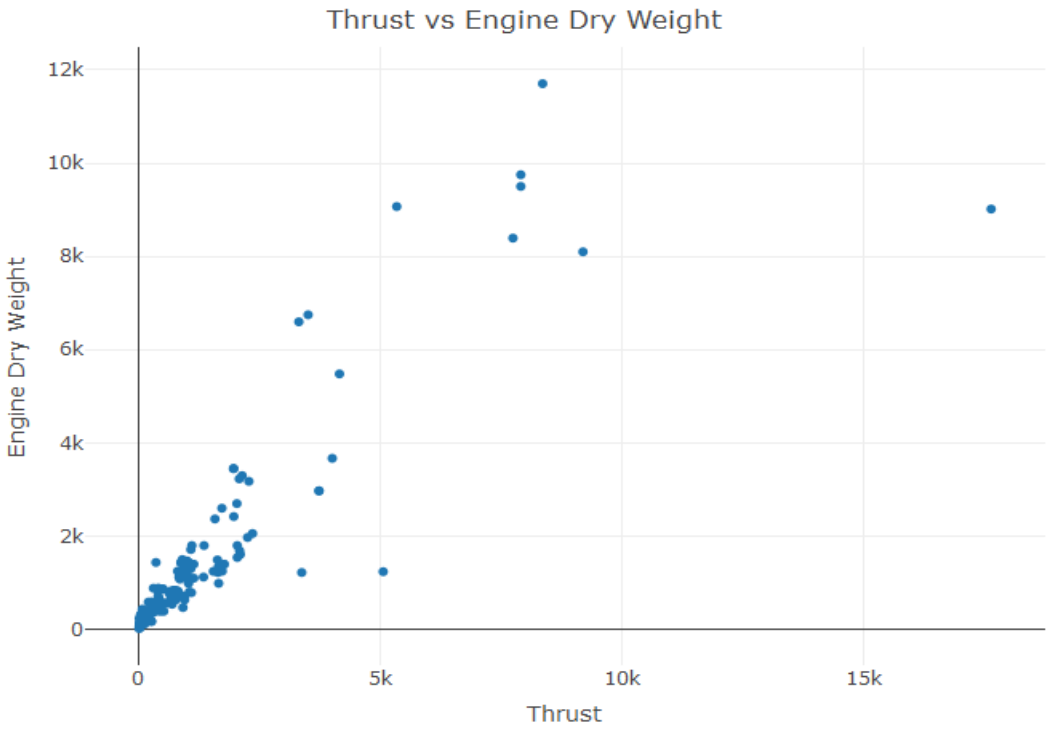

Figure 13: Scatter plot of Thrust and engine dry weight

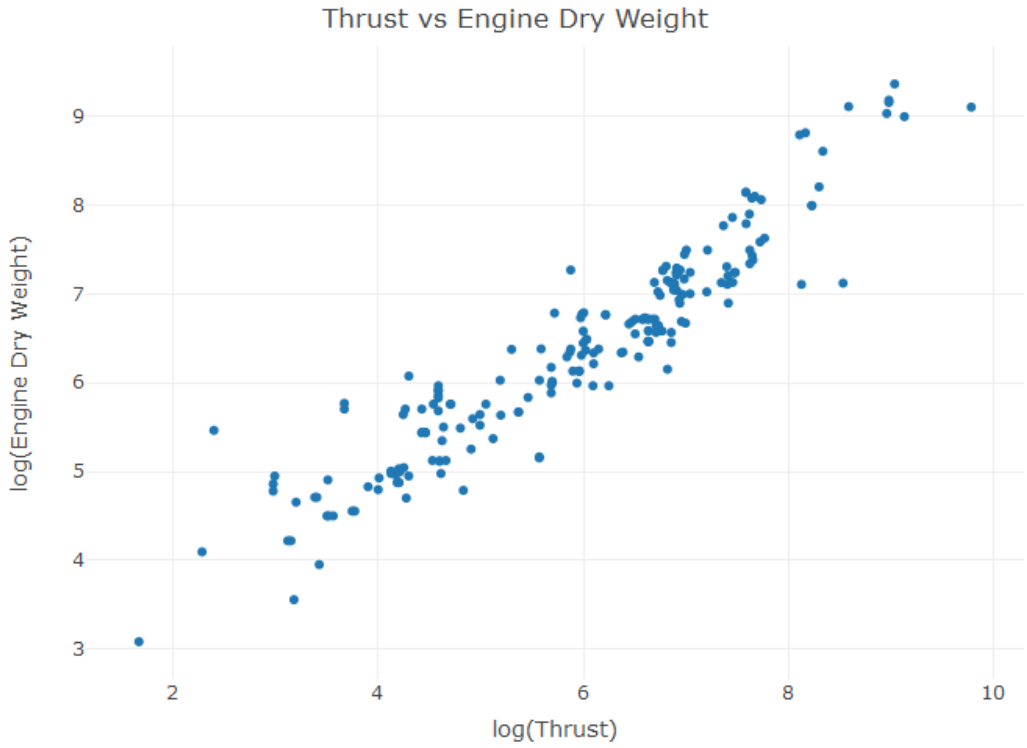

Figure 14: Scatter plot of thrust and engine dry weight on a logarithmic scale.

3.3.1 Correlation Test

To further confirm the relationship between thrust and weight a correlation test was run between the variables. The correlation between two variables can be found from their correlation coefficient which can be obtained from correlation analysis. There are different methods to perform a correlation analysis. Pearson correlation is used to measure the linear dependence between two variables. It is also known as a parametric correlation test because it depends on the distribution of the data [51]. It can be used only when two variables are from normal distribution. If the correlation coefficient is close to 1, it would indicate that the variables are positively linearly related, and the scatter plot falls almost along a straight line with positive slope (as seen in Figure 14). From the test, on a logarithmic scale the correlation coefficient between thrust and weight is 0.9284549 which shows how strongly the two variables are linearly related. Also, this means our data can be further analyzed through linear regression.

3.4 Linear Regression

Linear regression is used to predict the value of an outcome variable based on one or more input predictor variables. The aim is to model a linear relationship between two variables by fitting a linear equation to observed data. One variable is considered to be an explanatory variable, and the other is considered to be a dependent variable. Linear regression is the most commonly used type of predictive analysis. This mathematical equation can be generalized as follows:

$$Y = \beta_0 + \beta_1 * X + \varepsilon$$

Where, β_0 is the intercept and β_1 is the slope. In simple terms, they are the regression coefficients. ε is the error term, the part of Y the regression model is unable to explain [52-53].

Graphical analysis and correlation study in the previous sections have helped us in understanding the variables. Scatter plot, box plot and correlation test has helped in better

visualization of the data. From these we can conclude that the data is normally distributed and linearly correlated, thus ready for a regression model.

3.4.1 Weight ~ thrust linear model

In analysis not shown here, it was established that the relationship between thrust and weight is strongly log-log linear. Figure 15 represents a logarithmic scatter plot of thrust and weight with a linear fit to the data as determined from the regression analysis.

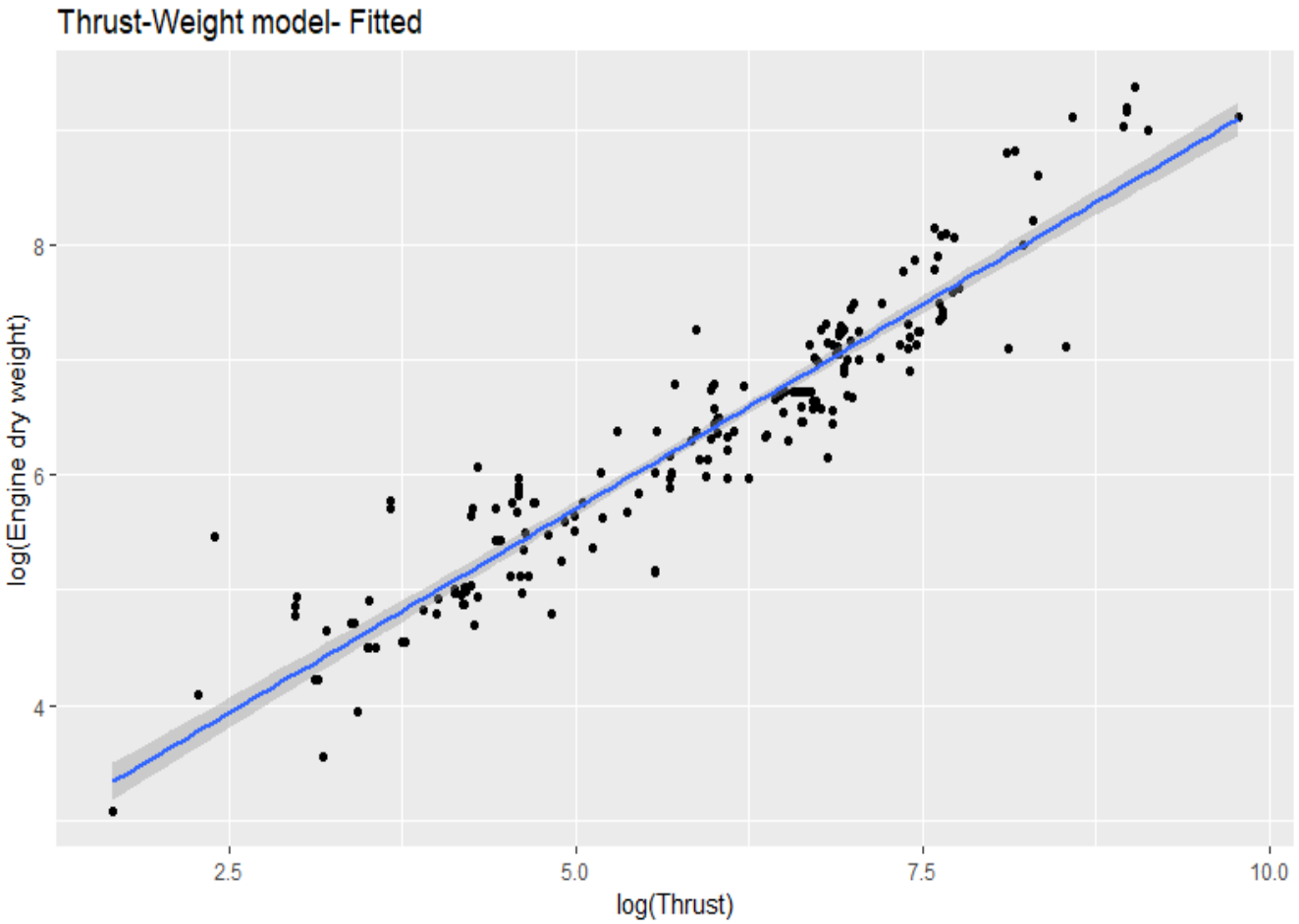

Figure 15: Weight as a function of thrust fitted with a regression line.

The coefficient of determination for this model is $R^2 = 0.8852$, which indicates a strong fit, i.e., 88.52% of the variability in log W is explained by its linear relationship to log T. This is a general linear model for all 211 data points of thrust and engine dry weight. Since it can explain 88.52% of variance in the data, the model is acceptable. The model can be further validated through

residual plots. Residual analysis plots are a very useful tool for assessing aspects of veracity of a linear regression model on a particular dataset and testing that the attributes of a dataset meet the requirements for linear regression.

General procedure after fitting a regression model is to check its residual plots [54-55]. Residual plots can help us check if we violate any assumptions of regression model. Residual values are displayed on the y axis and the fitted values are on the x axis. If the plots do not display any unwanted patterns, then our regression model is valid and the statistical values we obtain from it can be trusted. Figures 16 shows all the residual plots. In the first plot for residuals vs fitted values there are no underlying or obvious patterns. While it is slightly curved towards the right side the residuals are equally spread around the horizontal line without a distinct pattern. This is a good indication that the relationship between engine dry weight and thrust is nonlinear.

Residuals should be normally distributed in a Q-Q plot. If residuals follow close to straight line on this plot, it a good indication that they are normally distributed. For our model, the Q-Q plot shows good alignment to the line with few points at the top slightly offset. Scale location plot tests the linear regression assumption of equal variance (homoscedasticity) i.e. that the residuals have equal variance along the regression line. It is also called the spread-location plot. The residuals should occupy equal space above and below the line and along the length of the line. For our model the residuals are reasonably well spread above and below the horizontal line however there are fewer points with slightly less variance at the beginning of the line.

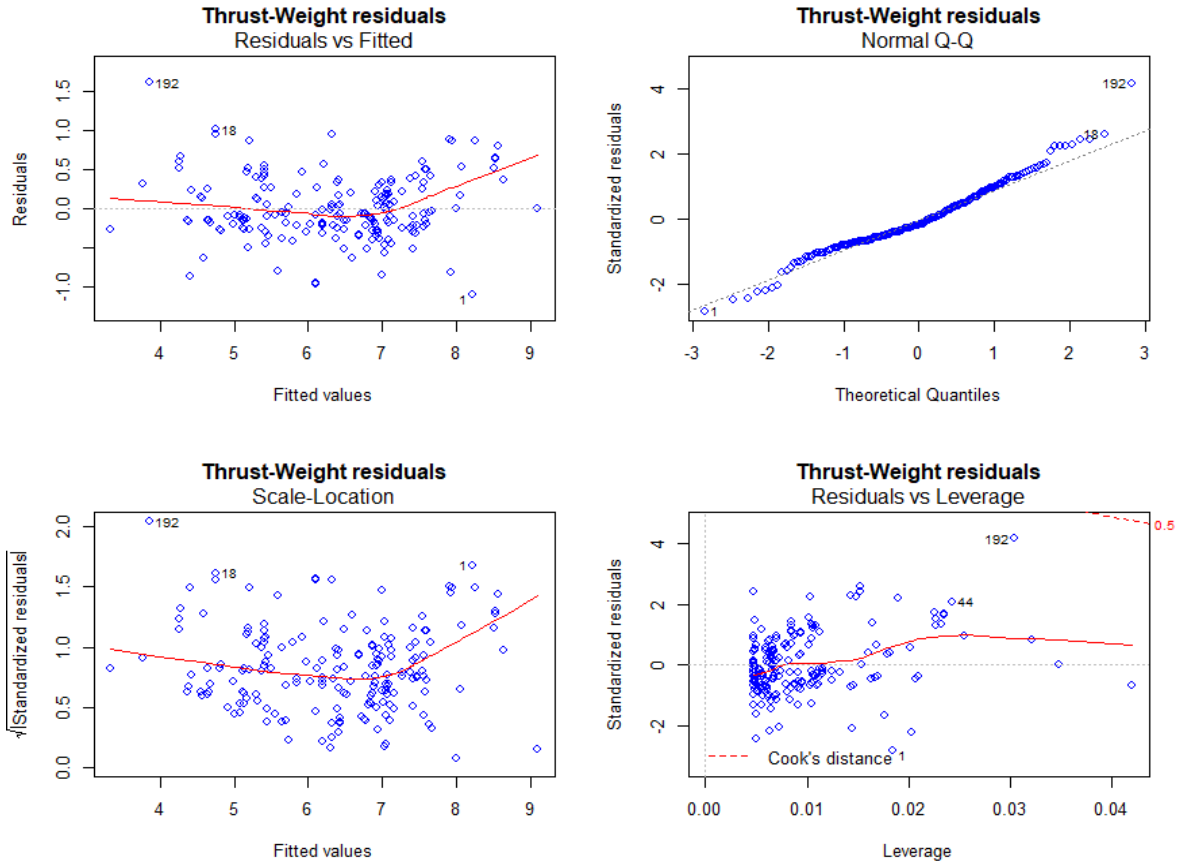

Figure 16: Residual plots of weight thrust linear model

Residuals vs Leverage plot can be used to find influential cases in the dataset. An influential case is one that, if removed, will affect the model so its inclusion or exclusion should be considered. An influential case may or may not be an outlier and the purpose of this chart is to identify cases that have high influence in the model. Outliers will tend to exert leverage and therefore influence the model. An influential case will appear in the top right or bottom left of the chart inside a red line which marks Cook's Distance. Our model does not have any point inside this line however there is one point that is away from the rest of the data cluster. Upon further exploring the residual plots, the data points (18,44,121,122,124,192) has been found to have some influence on the model. Referring back to the data set revealed these data points to be containing extreme values which automatically make them outliers. The model was updated by removing

these datapoints and the coefficient of determination R^2 increased to 0.898 which means the model can now explain 89.8% variability in the data. Clearly there are no heteroscedasticity or recognizable patterns in our residual plots. This means the general linear regression model built for engine dry weight and thrust is valid. A histogram of residuals from a linear model should show a normal distribution of residuals which is verified from figure 17 showing the residual histogram for our linear model.

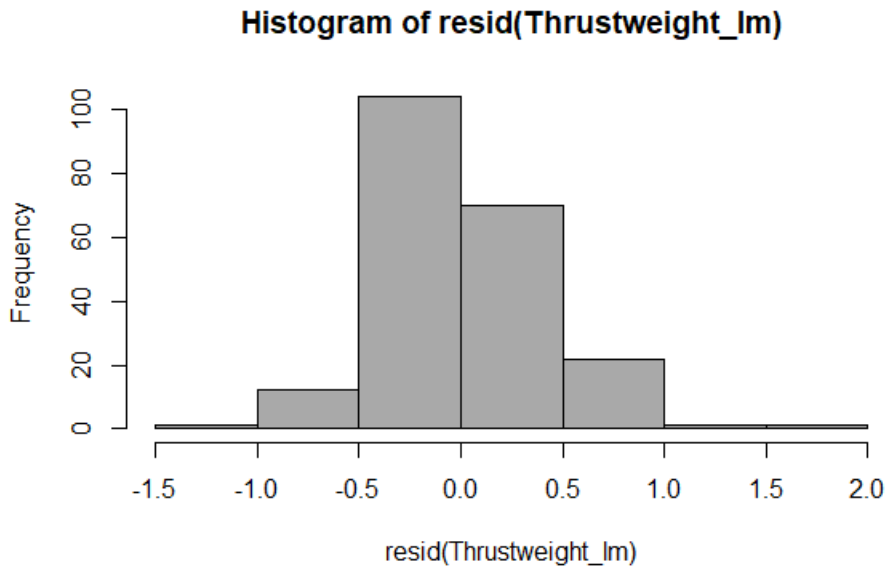

Figure 17: Histogram of residuals.

Thus, the regression analysis on the log values resulted in the following log-log linear model:

$$\log W = 2.05995 + 0.72328 * \log T \quad (1)$$

By exponentiation of both sides of the equation (1), the following non-linear relationship is established between thrust and weight,

$$W = 7.84558 * T^{0.72328} \quad (2)$$

An interesting attribute about the dataset is that the performance variables can be grouped based on cycles as seen earlier in data visualization through boxplots based on cycles. Since they don't have comparable amount of data points they can't be modelled individually as the results based on fewer data points cannot be relied upon. So, the dataset is kept as a whole, and a multiple linear regression model is developed based on engine power cycles. Multiple linear regression is an extension of linear regression which attempts to model the relationship between two or more explanatory variables and a response variable by fitting a linear equation to observed data. Every value of the independent variable x is associated with a value of the dependent variable y. This mathematical equation can be generalized as follows:

$$Y = \beta_0 + \beta_1 * X_1 + \beta_2 * X_2 + \beta_3 * X_3 + \beta_4 * X_4 + \ldots\ldots\ldots + \varepsilon$$

Where β terms are the regression coefficients, X terms are the predictor variable, Y is the response variable and ε is the error term [56].

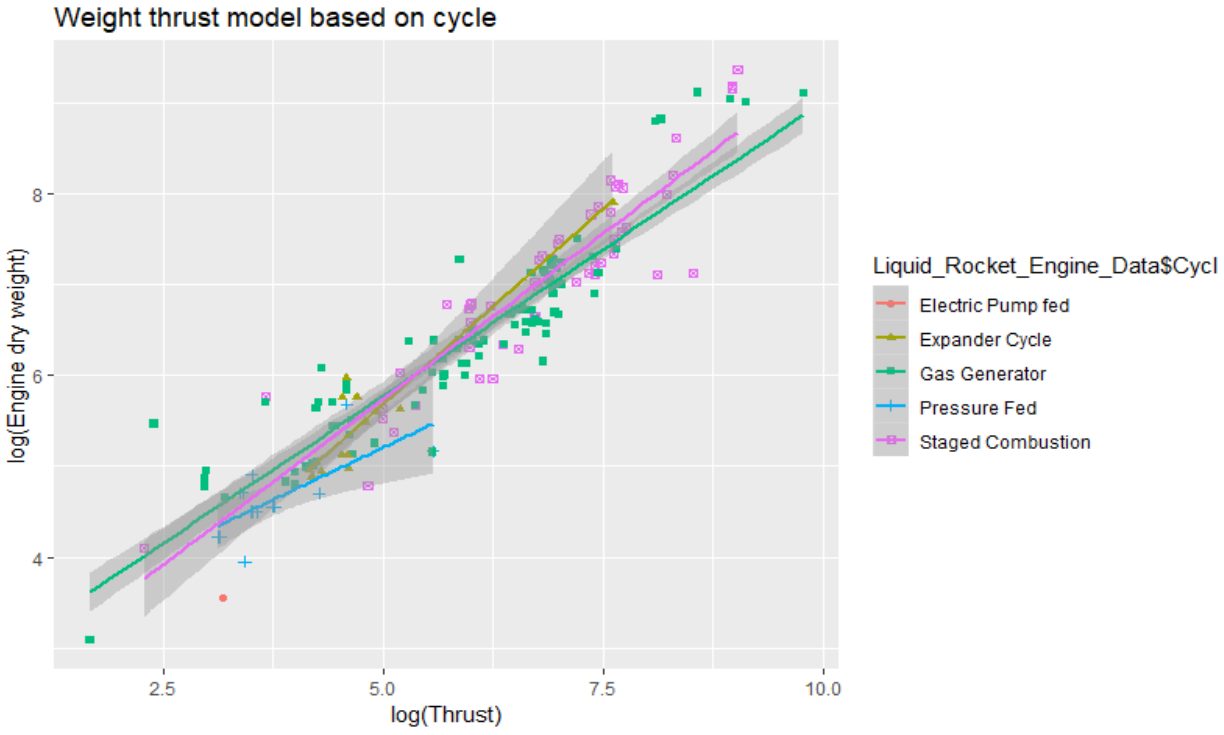

Figure 18: Engine dry weight as a function of thrust based on cycle.

Similar procedure is followed as in a simple linear regression model and the following fit is obtained as shown in figure 18. The data is modelled as a whole, and a fit is generated in a single plot for different cycles. The coefficient of determination for this model is $R^2 = 0.8904$, which indicates a strong fit, i.e., 89.04% of the variability in log W is explained by its linear relationship to log T based on engine cycle. General procedure after fitting a regression model is to check its residual plots. To validate the model as we did for the general regression model for the dataset we rely on residual plots. The residual plots for the regression model based on cycle is shown in figure 19. In the first plot for residuals vs fitted values there are no underlying or obvious patterns. While it is slightly curved towards the right side, the residuals are equally spread around the horizontal line without a distinct pattern.

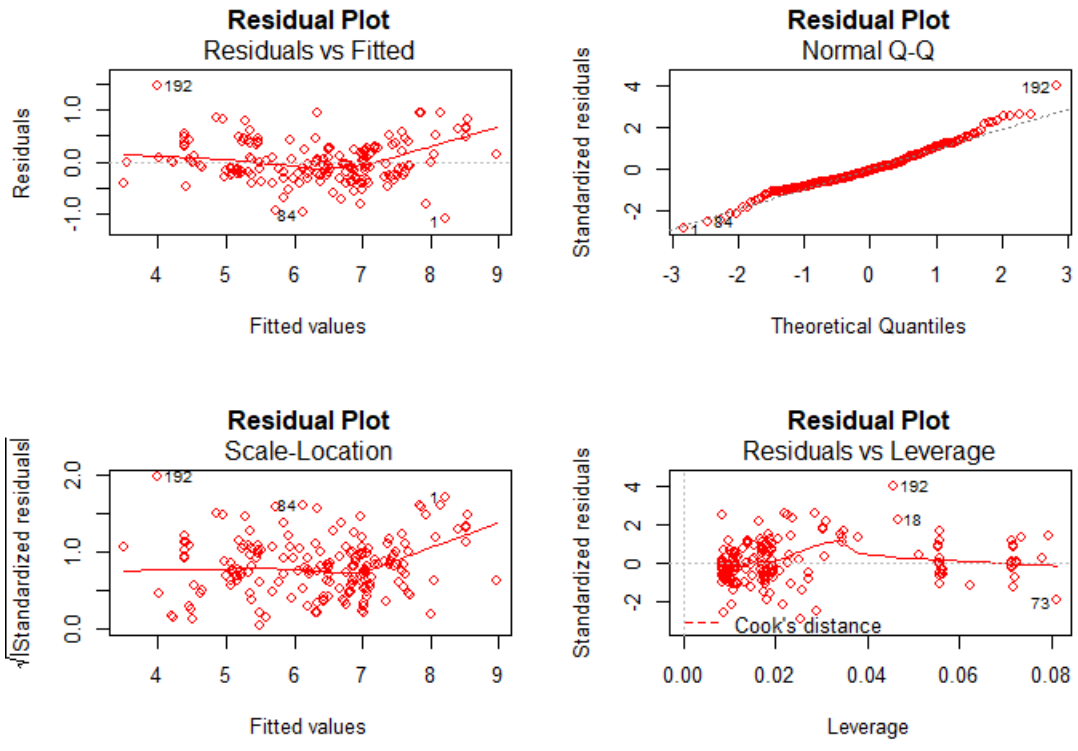

Figure 19: Residual plots for multi regression based on engine cycle.

Residuals should be normally distributed in a Q-Q plot. If residuals follow close to straight line on this plot, it a good indication that they are normally distributed. For our model, the Q-Q plot shows good alignment to the line with few points at the top right slightly offset. Scale location plot tests the linear regression assumption of equal variance (homoscedasticity) i.e. that the residuals have equal variance along the regression line. It is also called the spread-location plot. The residuals should occupy equal space above and below the line and along the length of the line. For our model the residuals are reasonably well spread above and below the horizontal line however there are fewer points with slightly less variance at the beginning of the line.

Residuals vs Leverage plot can be used to find influential cases in the dataset. An influential case is one that, if removed, will affect the model so its inclusion or exclusion should be considered. An influential case may or may not be an outlier and the purpose of this chart is to identify cases that have high influence in the model. Outliers will tend to exert leverage and therefore influence the model. An influential case will appear in the top right or bottom left of the chart inside a red line which marks Cook's Distance. Our model does not have any point inside this line however there are couple of points that are away from the rest of the data cluster. Upon further exploring the residual plots, the data points (18,28,27,73,104,106,192) has been found to have some influence on the model. Referring back to the data set revealed these data points to be containing extreme values which automatically make them outliers. The model was updated by removing these datapoints and the coefficient of determination R^2 increased to 0.906 which means the model can now explain 90.6% variability in the data. There are no heteroscedasticity or recognizable patterns in our residual plots. This means the multi linear regression model built for engine dry weight and thrust based on cycle is valid. A histogram of residuals from a linear model

should show a normal distribution of residuals which is verified from figure 20 showing the residual histogram for our linear model.

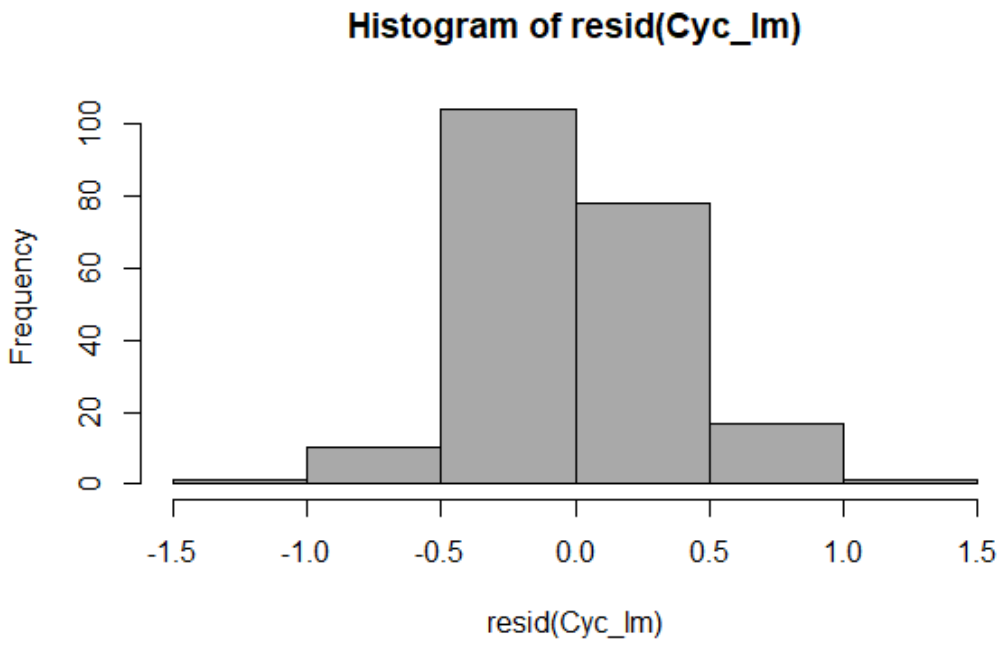

Figure 20: Histogram of Residuals

The regression analysis on the logarithmic data split based on cycles resulted in a log-log linear model which can be interpreted and classified into sub models representing each engine cycle. The equations from the sub model for each engine cycle is represented in the following general form as shown in Table 4.

Table 4: General form of Sub model for engine cycles

Engine Cycle	General Equation
Expander Cycle	Log W = $(\beta_0 + \beta_2) + \beta_1$ *log (Thrust)
Gas Generator Cycle	Log W = $(\beta_0 + \beta_3) + \beta_1$ *log (Thrust)
Pressure Feed Cycle	Log W = $(\beta_0 + \beta_4) + \beta_1$ *log (Thrust)
Staged Combustion Cycle	Log W = $(\beta_0 + \beta_5) + \beta_1$ *log (Thrust)

Table 5: Coefficient value for each cycle

	Coefficient	Estimate
Intercept	β_0	1.33361
Thrust	β_1	0.69909
Expander	β_2	0.81822
Gas generator	β_3	0.88178
Pressure feed	β_4	0.73538
Staged combustion	β_5	0.97164

Table 5 summarizes the coefficient values for each cycle which can be substituted in the general equation. This will give us an equation to predict engine dry weight based on a given cycle. By exponentiation of both sides of the equation in Table 4, the following non-linear relationship is established between thrust and weight based on cycle as shown in Table 6. The equation obtained from the model can be used to predict engine dry weight for a given thrust.

Table 6: Equations to predict weight for a given thrust based on engine cycle.

Engine Cycle	Logarithmic Equation	Predictive Equation
Expander Cycle	Log W = (1.33361+ 0.81822)+ 0.69909*log (Thrust)	$W = 8.60058*Thrust^{0.69909}$
Gas Generator Cycle	Log W = (1.33361+ 0.88178)+ 0.69909*log (Thrust)	$W = 9.16498*Thrust^{0.69909}$
Pressure Feed Cycle	Log W = (1.33361+ 0.73538)+ 0.69909*log (Thrust)	$W = 7.91682*Thrust^{0.69909}$
Staged Combustion Cycle	Log W = (1.33361+ 0.97164)+ 0.69909*log (Thrust)	$W = 10.0267*Thrust^{0.69909}$

3.5 Predictive Modeling

Predictive modeling is the process of building a model to predict future outcomes using statistical techniques [57-58]. The model is setup by creating a training data set and testing data set. The training data set consists of the 80% of the data from our dataset and is used to develop the model. The model is setup in such a way that it chooses the same random data every time which helps us in maintaining a constant dataset. Remaining 20% of the data constitutes the test data set which are solely used for evaluating the performance of the model. Regression model between engine dry weight and thrust is built using the training dataset. This regression model is similar to the model we built in the previous section and can be verified in the similar way. Figure 21 shows a linear model fitted to our training data.

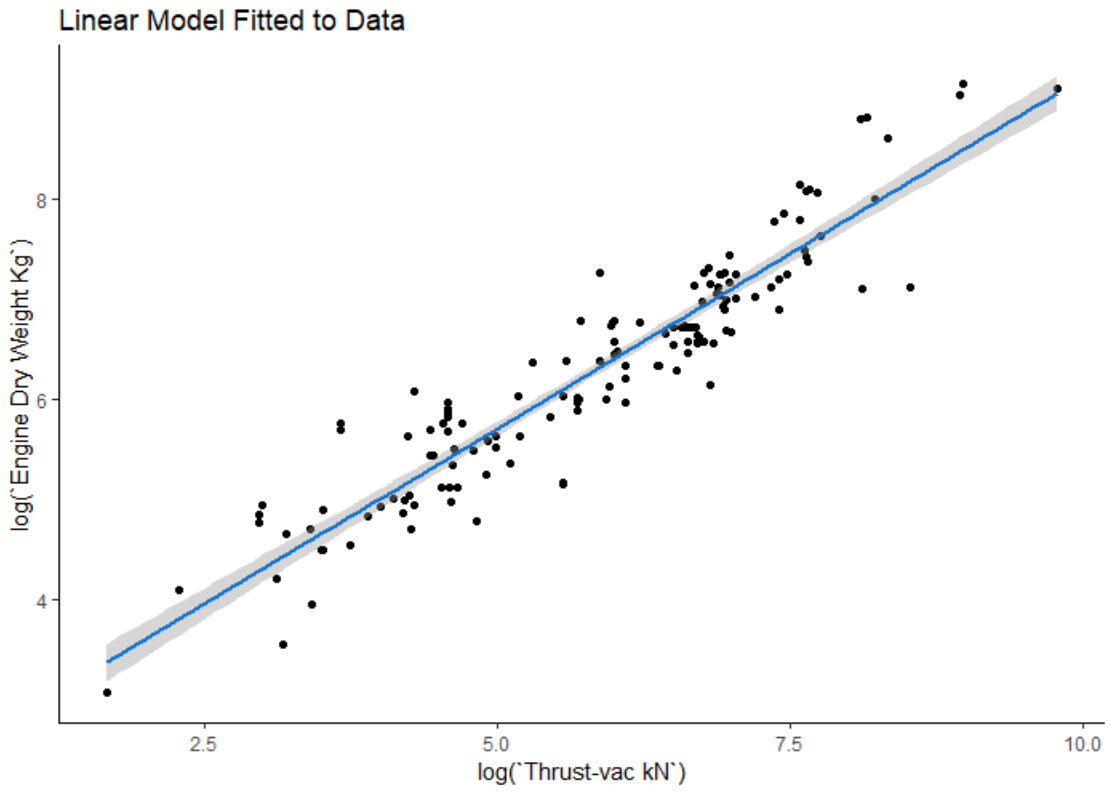

Figure 21: Linear model fitted to training set.

The coefficient of determination for this model is $R^2 = 0.8778$, which indicates a strong fit, i.e., 87.78% of the variability in our dataset is explained by the model. Similar to previous sections the residuals of the model can be checked to validate it further. From figure 22 we can clearly see that there are no patterns in our data, and it spread relatively evenly along the horizontal. Normal Q-Q plot shows that the distribution is normal. Histogram of residuals from figure 23 confirms normal distribution as we can see clearly a normal distribution of residuals around zero and the model can be used to proceed further. There are no anomalies in our model, and this can be used for predicting engine dry weight.

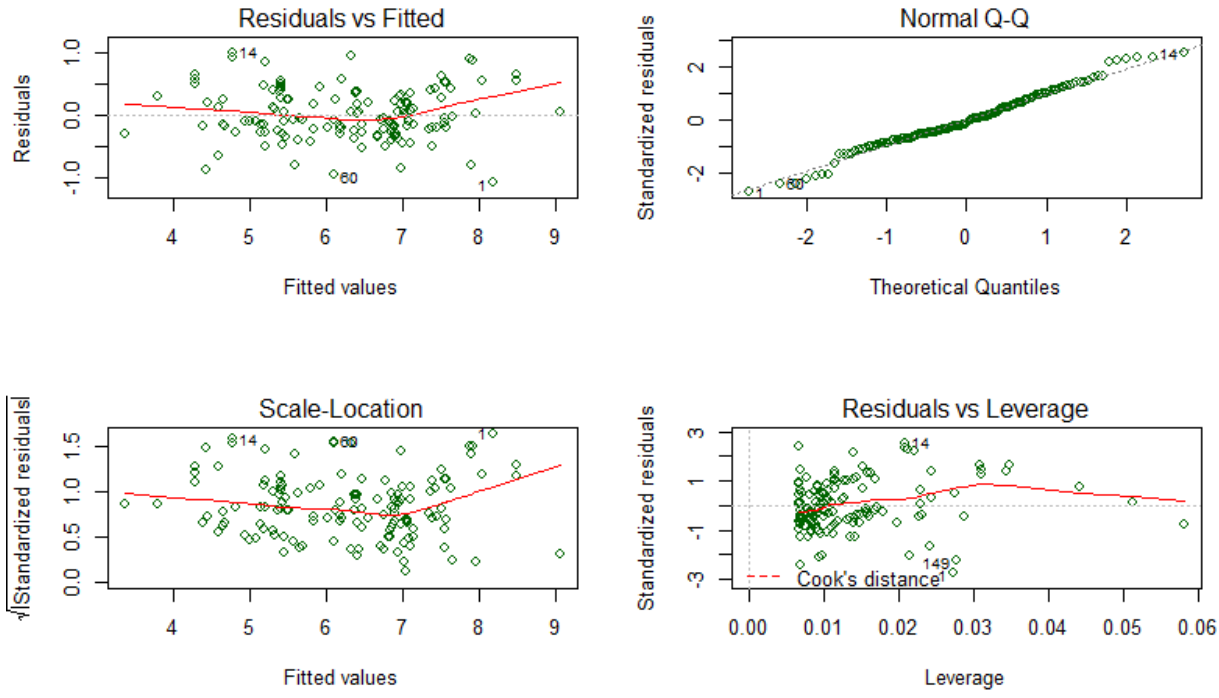

Figure 22: Residuals of training data

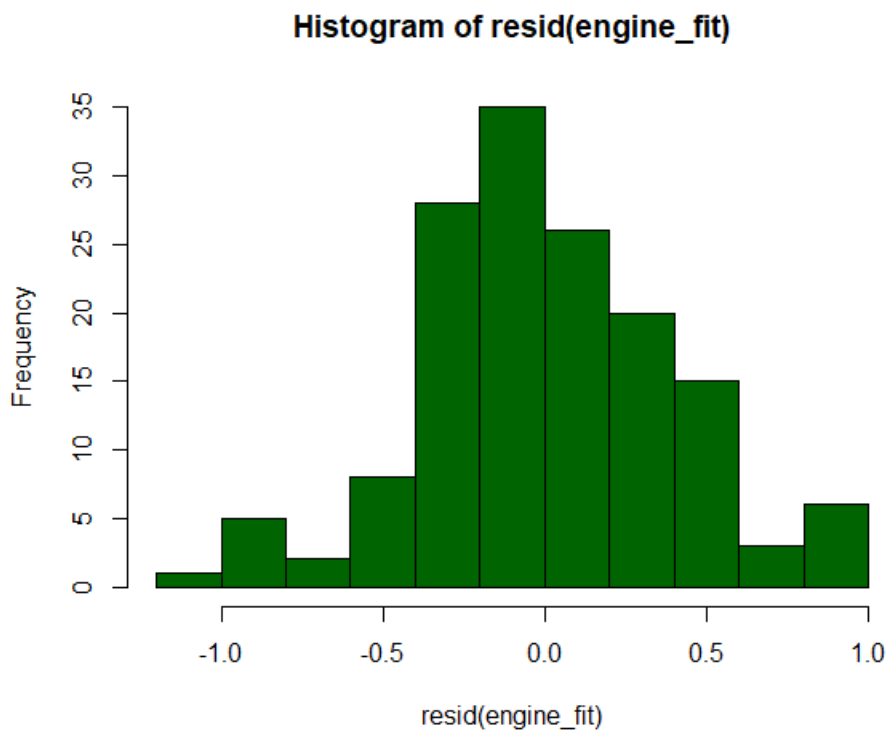

Figure 23: Histogram of residuals for training data.

Now the remaining 20% of data in the testing set is used to make the prediction based on the above model. This will reveal the accuracy of the model we built. A linear fit to the predictive model produced a coefficient of determination R^2 of 0.9009 which implies the model can explain 90.09% of variance in the data and its prediction is quite accurate. Since our model is log based the predicted values are log based as well. This value can be exponentiated to find out the actual value of engine dry weight. Predicted value and the actual values is plotted as shown in figure 24 to check for linear spread of data. As we can see the data is spread linearly

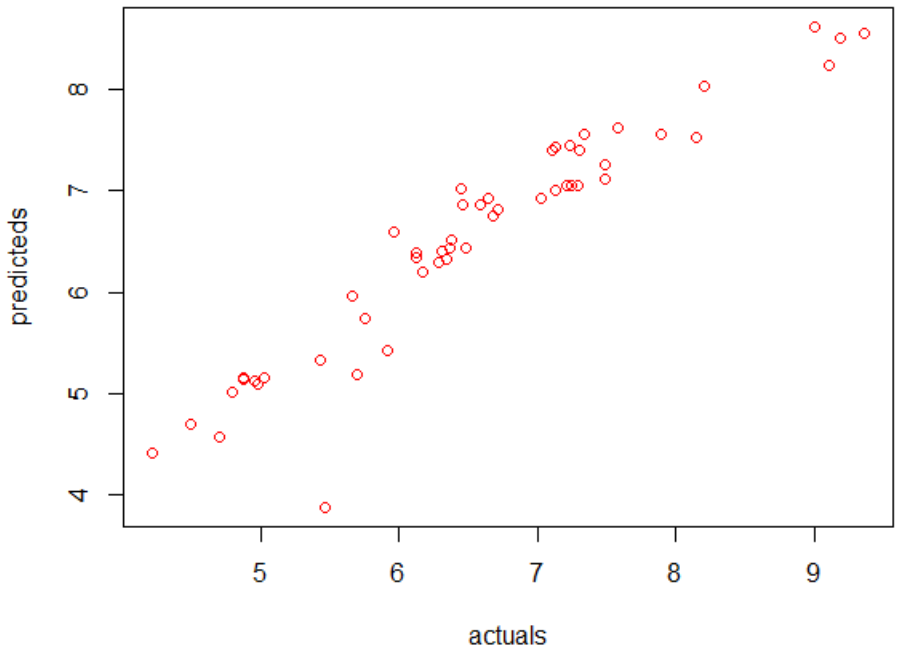

Figure 24: Actual value vs Predicted value

There are couple of other methods to estimate the accuracy and error percentage of our predictive model. Min/Max accuracy will find out the accuracy of each row. It takes for each row the ratio of minimum and maximum of the prediction result. For a perfect model this measure is 1. Taking the mean of this measure over the entire model gives us the accuracy rate of each row which can be considered the accuracy rate of the model. Our predictive model has a min/max accuracy of 0.9582 or our model prediction is 95.82% accurate. Mean absolute percentage error is the average of absolute percentage errors which is the measure of the prediction accuracy of a model. MAPE value for our model is 0.04279 or 4.28% which indicates our model has an error percentage of 4.28% in its prediction of engine dry weight.

Similar model is built based on cycles. Regression model between engine dry weight and thrust is built using the training dataset. Figure 25 shows a linear model fitted to our training data.

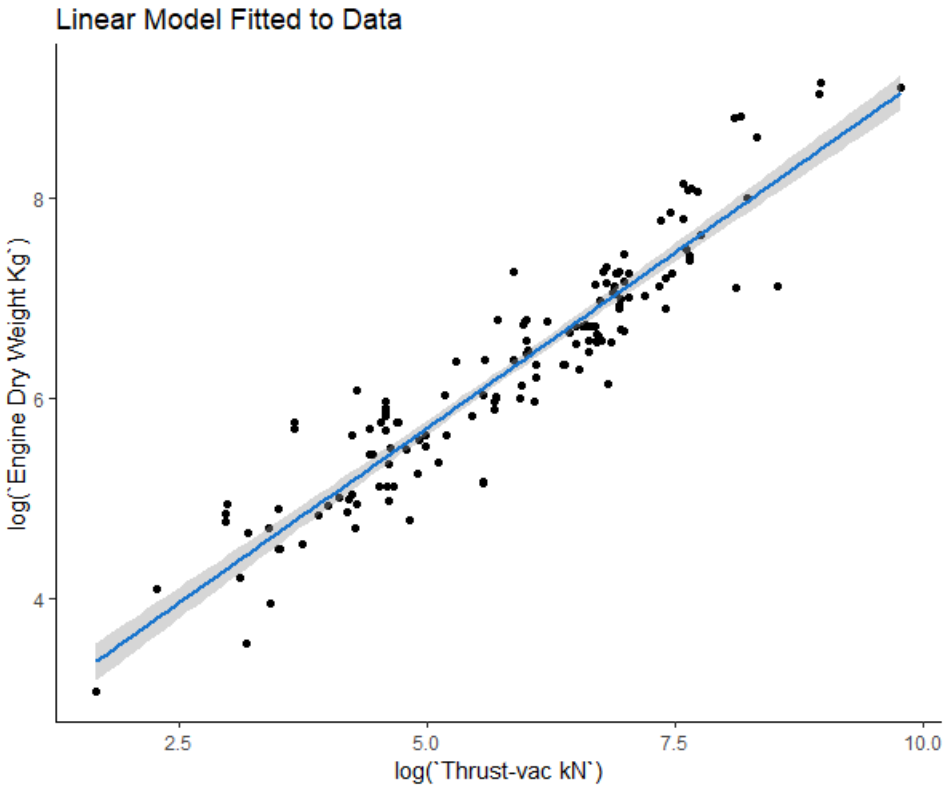

Figure 25: Linear model fitted to training set based on cycles.

The coefficient of determination for this model is $R^2 = 0.8858$, which indicates a strong fit, i.e., 88.58% of the variability in our dataset is explained by the model. Similar to previous sections the residuals of the model can be checked to validate it further. From figure 26 we can clearly see that there are no patterns in our data, and it is spread relatively evenly along the horizontal. Normal Q-Q plot shows that the distribution is normal. Histogram of residuals from figure 27 confirms normal distribution as we can see clearly a normal distribution of residuals around zero and the model can be used to proceed further. There are no anomalies in our model, and this can be used for predicting engine dry weight.

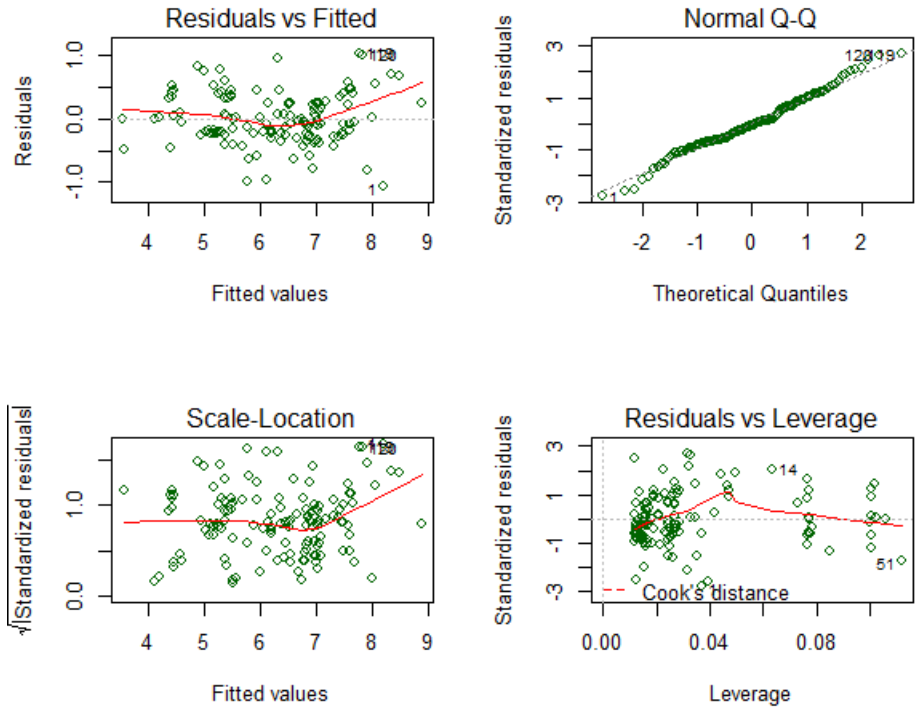

Figure 26: Residuals of training data.

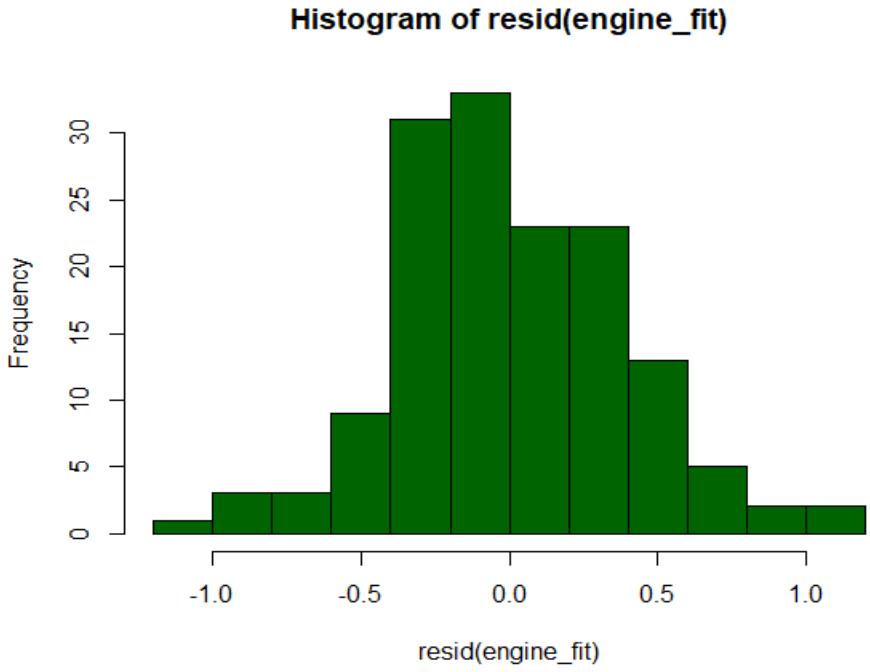

Figure 27; Histogram of Residuals

Our predictive model has a coefficient of determination $R^2 = 0.899$ for the test data which explains 89.9% of the variability. Model has a min/max accuracy of 0.95867 or our model prediction is 95.87% accurate. Mean absolute percentage error is the average of absolute percentage errors which is the measure of the prediction accuracy of a model. MAPE value for our model is 0.04237 or 4.24% which indicates our model has an error percentage of 4.24% in its prediction of engine dry weight.

3.5.1 k-fold Cross Validation

Determining the accuracy or prediction error of the model on predicting the outcome for new unseen observation is a good way to check the performance of the model. Cross validation is a technique to evaluate a predictive model by partitioning the original data into training set to train the model and a test set to evaluate it. In a k-fold cross validation, the original sample is partitioned into k equal sizes. A single subsample is retained as the validation data for testing the model and remaining k-1 subsamples are used as training data. The cross-validation process is repeated k times with each of k subsamples and exactly once on the validation data. K results from the folds are averaged to produce a single estimation. Advantage of this method is that all observations are used for both training and validation, and each observation is used for validation exactly once [59-60].

R-squared, Root Mean Squared Error (RMSE) and Mean Absolute Error (MAE) are used to measure the regression model performance during cross validation. The main goal of cross validation here is to make sure the data is not overfitted or underfitted. 10-fold cross validation of the simple linear model produced a R-squared of 0.8926, RMSE of 0.3894 and MAE of 0.30386. For the model based on cycle the R-squared was 0.9004, RMSE was 0.382 and MAE was 0.3018.

Generally, the R-squared value should be as high as possible, RMSE and MAE values should be as low as possible. There is no overfitting of data in either model and the linear model based on cycle is slightly better based on the validation result.

3.6 Quadratic Model

It is always in our curiosity to find better things. Though our linear model has a good performance there is always room for improvement. So, we'll see if a quadratic model fits our data better. The model is setup in similar ways to a linear model that in it is essentially a linear model in two variables, one of which is the square of the other. We used the thrust term to predict weight in our linear model [61-63]. In addition to this we include a thrust^2 term to our linear model which makes it a quadratic model. The equation of such regression is of the following form:

$$Y = \beta_0 + \beta_1 * X_1 + \beta_2 * X_1^2$$

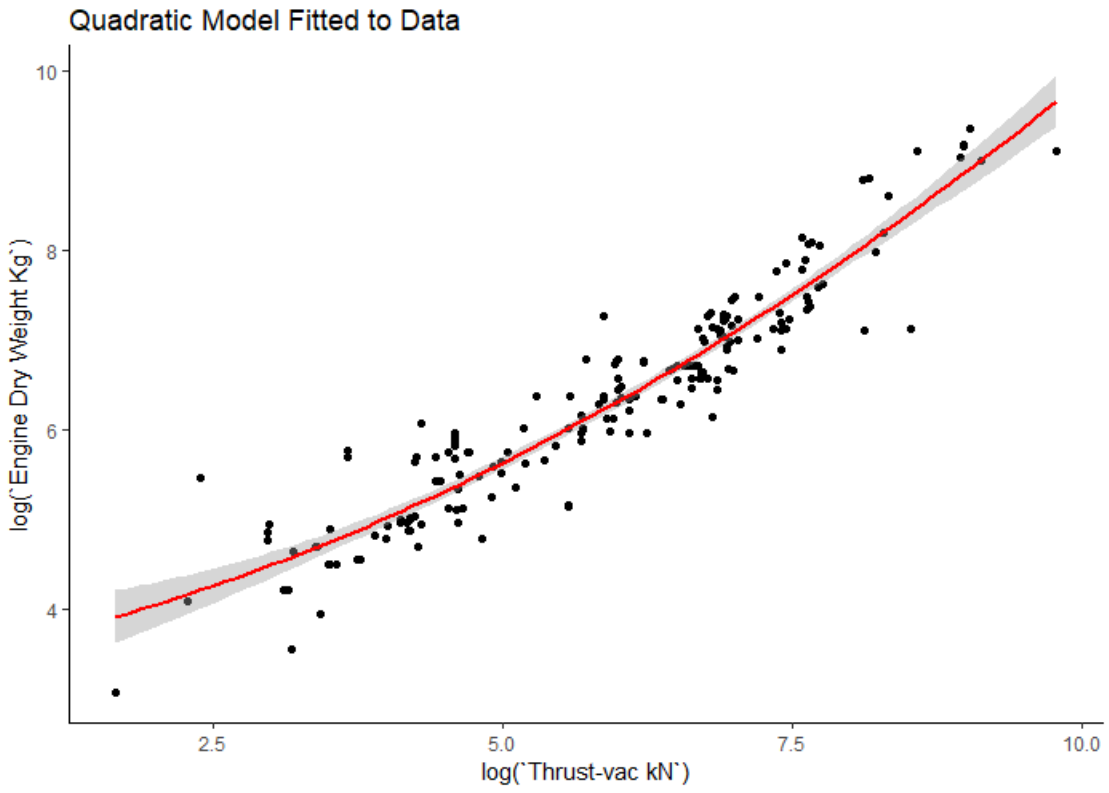

Figure 28: Quadratic fit for engine dry weight and thrust regression model

A quadratic fit to our data is shown in figure 28. This model is similar to the first regression model where the fit was made to all the data points. The coefficient of determination R^2 for our model with a quadratic fit is 0.8948 or it can explain 89.48% of variance between engine dry weight and thrust. This value is slightly better than the linear model. The model can be further validated by checking the residual plots shown in figure 29. The equation to predict weight from the model is as follows:

$$\text{Log W} = 3.402858 + 0.242749 * \log \text{Thrust} + 0.040654 * (\log (\text{Thrust}))^2$$

Based on logarithmic power rule the above equation can be simplified.

$$\text{Log W} = 3.402858 + 0.242749 * \log \text{Thrust} + 0.040654 * (\log (\text{Thrust}))^2$$

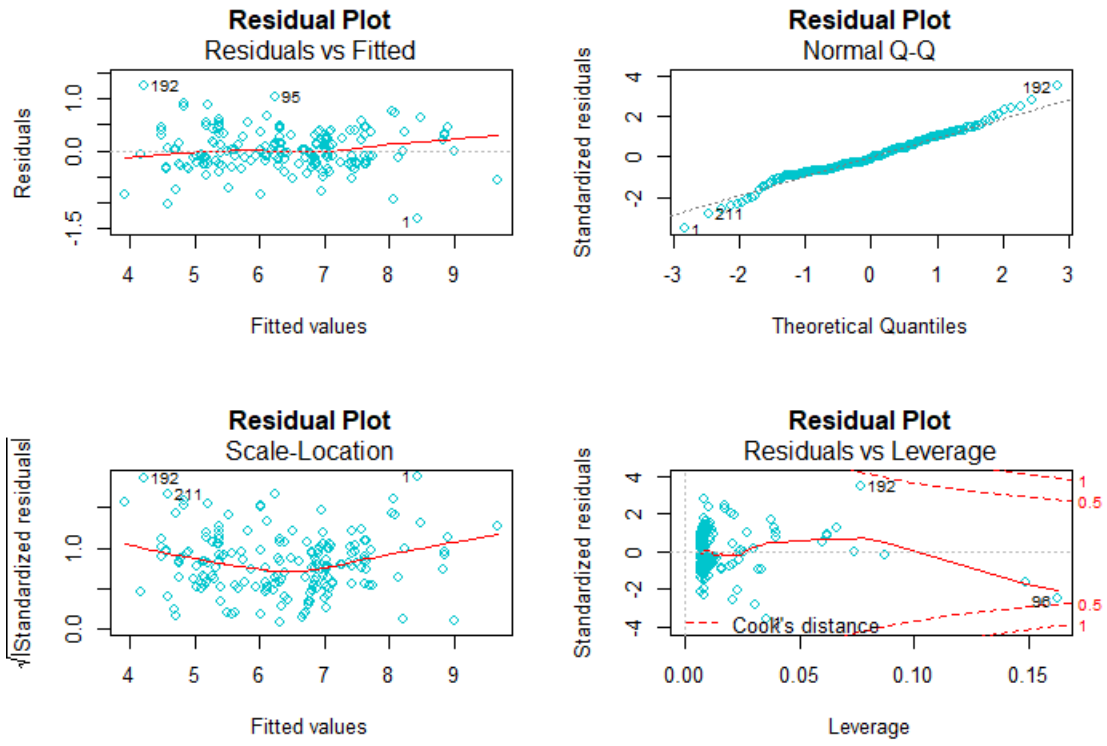

Figure 29: Residual plots of quadratic model

Residuals should be normally distributed in a Q-Q plot. If residuals follow close to straight line on this plot, it a good indication that they are normally distributed. For our model, the Q-Q plot shows good alignment to the line with few points at the top right and bottom left slightly offset. Scale location plot tests the linear regression assumption of equal variance (homoscedasticity) i.e. that the residuals have equal variance along the regression line. The residuals should occupy equal space above and below the line and along the length of the line. For our model the residuals are reasonably well spread above and below the horizontal line however there are fewer points with slightly less variance.

Residuals vs Leverage plot can be used to find influential cases in the dataset. An influential case is one that, if removed, will affect the model so its inclusion or exclusion should be considered. An influential case may or may not be an outlier and the purpose of this chart is to identify cases that have high influence in the model. Outliers will tend to exert leverage and therefore influence the model. An influential case will appear in the top right or bottom left of the chart inside a red line which marks Cook's Distance. Our model does not have any point inside this line however there are couple of points (96 and 192) that are very close to the Cook's Distance line. These two points could have slight influence on the model. Our dataset is such that contains extremities of data as explained earlier. So, this influence is neglected as our model has a satisfactory performance. Goodness of our model can be verified from the histogram shown in figure 30 as it shows a normal distribution of residuals around zero.

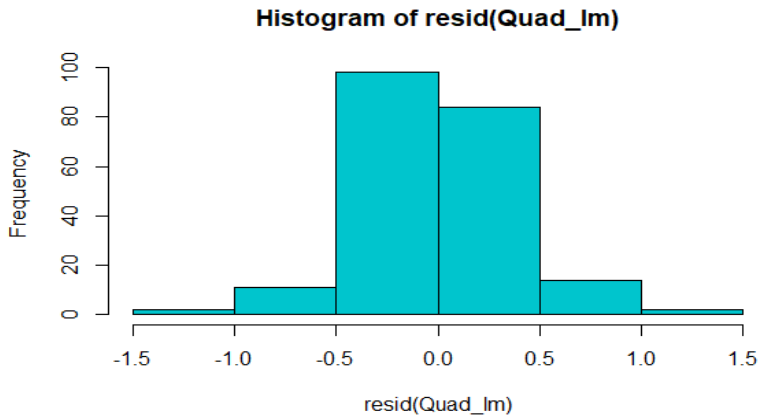

Figure 30: Histogram of residuals for quadratic model.

As we did in linear regression model the dataset can be sub-grouped into engine cycles to perform a multiple regression analysis. In this case it is going to be a multiple quadratic regression analysis. Quadratic fit for our model based on engine cycle is shown in figure 31. The equations from the sub model for each engine cycle is represented in the following general form as shown in Table 7.

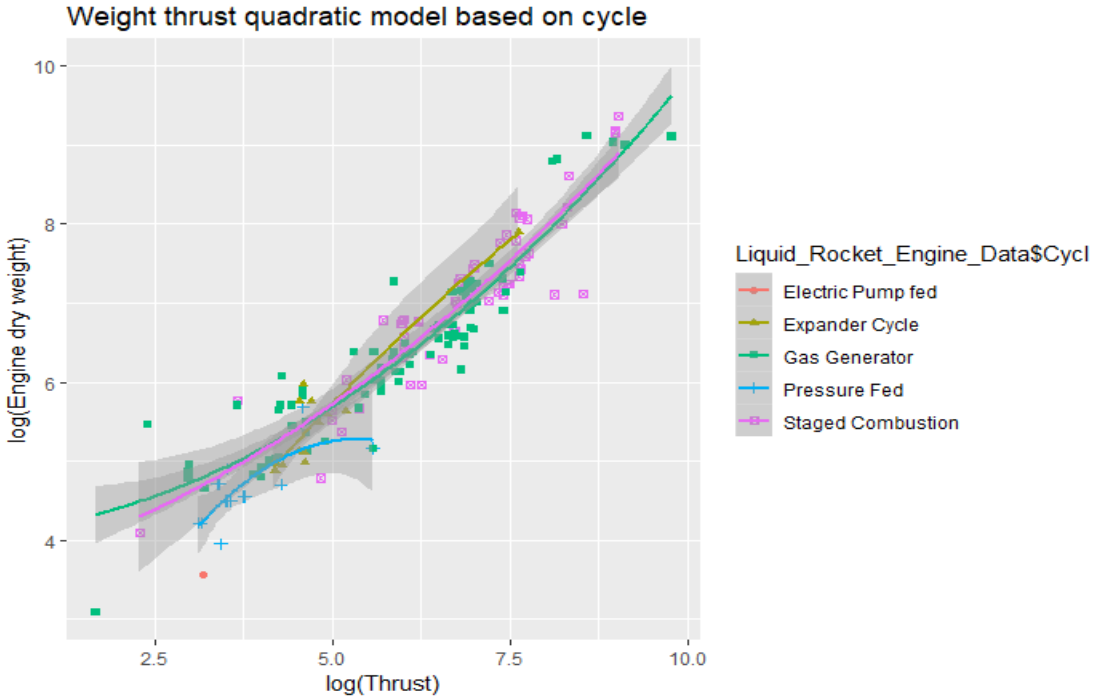

Figure 31: Quadratic model based on engine cycle.

Table 7: General form equations from quadratic model based on engine cycle

Engine Cycle	General Equation
Expander Cycle	$\text{Log } W = (\beta_0 + \beta_3) + \beta_1 * \log(\text{Thrust}) + \beta_2 * (\log(\text{Thrust}))^2$
Gas Generator Cycle	$\text{Log } W = (\beta_0 + \beta_4) + \beta_1 * \log(\text{Thrust}) + \beta_2 * (\log(\text{Thrust}))^2$
Pressure Feed Cycle	$\text{Log } W = (\beta_0 + \beta_5) + \beta_1 * \log(\text{Thrust}) + \beta_2 * (\log(\text{Thrust}))^2$
Staged Combustion Cycle	$\text{Log } W = (\beta_0 + \beta_6) + \beta_1 * \log(\text{Thrust}) + \beta_2 * (\log(\text{Thrust}))^2$

The coefficient of determination for this model is $R^2 = 0.9036$, which indicates a strong fit, i.e., 90.36% of the variability in log W is explained by its linear relationship to log T based on engine cycle. The residual plots for the regression model based on cycle is shown in figure 32. In the first plot for residuals vs fitted values there are no underlying or obvious patterns. While it is slightly curved towards the right side, the residuals are equally spread around the horizontal line without a distinct pattern. Residuals should be normally distributed in a Q-Q plot. If residuals follow close to straight line on this plot, it a good indication that they are normally distributed. For our model, the Q-Q plot shows good alignment to the line with few points at the top right slightly offset. Scale location plot tests the linear regression assumption of equal variance (homoscedasticity) i.e. that the residuals have equal variance along the regression line. The residuals should occupy equal space above and below the line and along the length of the line. For our model the residuals are reasonably well spread above and below the horizontal line however there are fewer points with slightly less variance at the beginning of the line.

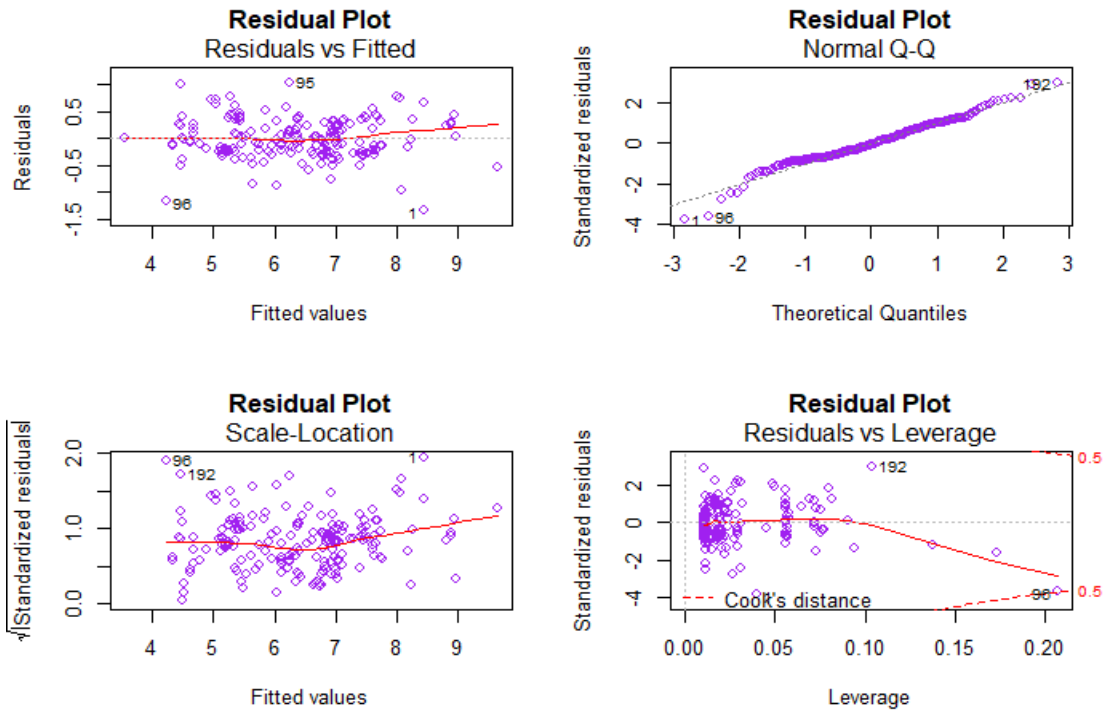

Figure 32: Residual plots for quadratic model based on cycle

Residuals vs Leverage plot can be used to find influential cases in the dataset. An influential case is one that, if removed, will affect the model so its inclusion or exclusion should be considered. An influential case may or may not be an outlier and the purpose of this chart is to identify cases that have high influence in the model. Outliers will tend to exert leverage and therefore influence the model. An influential case will appear in the top right or bottom left of the chart inside a red line which marks Cook's Distance. Our model does not have any point inside this line however there is a point that is almost on the Cook's Distance line and two more points which are away from the data cluster. These points could have some effect on our model. Hence all three points (1,96,192) were excluded from the regression model. The coefficient of determination R^2 increased slightly to 0.9157 i.e. the model can explain 91.57% of variance in our data which is a very good fit. The new residual plot is shown in figure 33 has no deviations and the residuals are verified by histogram of residuals as shown in figure 34.

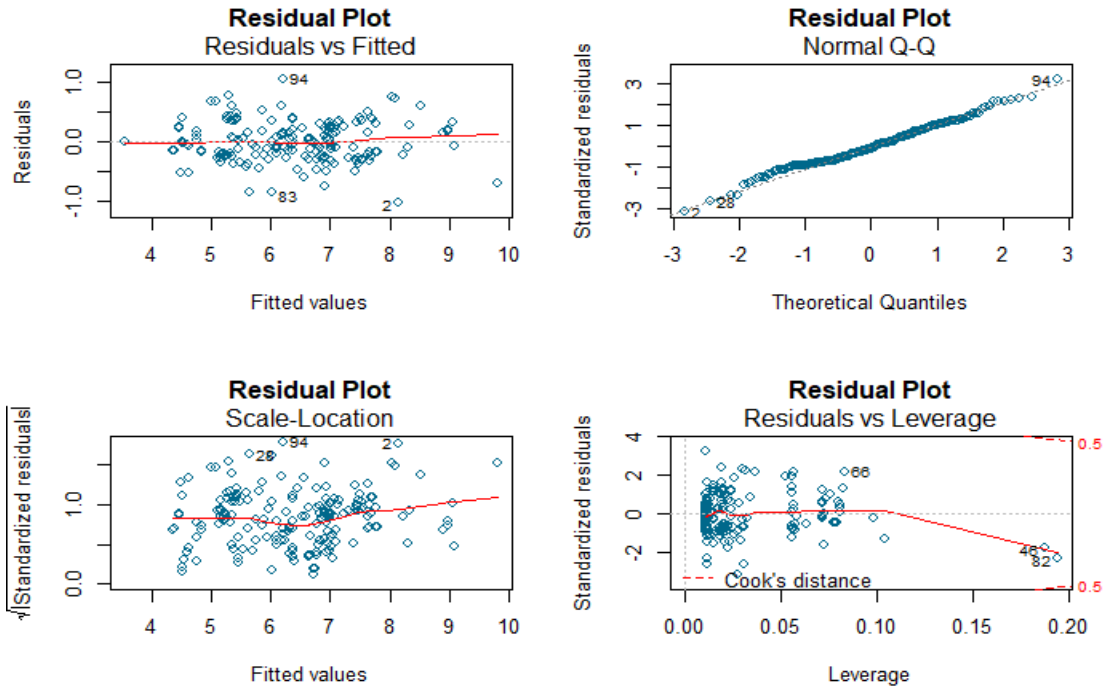

Figure 33: Residuals of refined quadratic model.

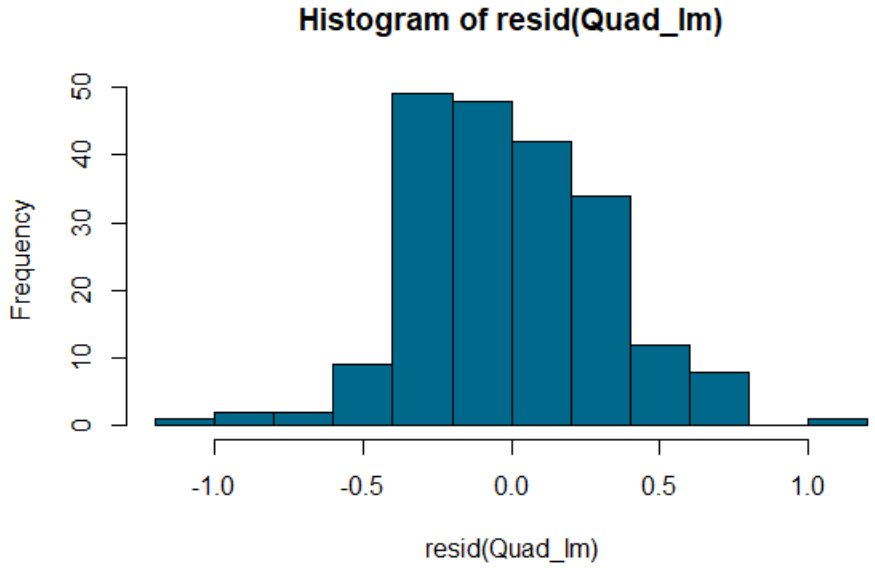

Figure 34: Histogram of residuals.

Table 8: Coefficient value for each cycle

	Coefficient	Estimate
Intercept	β_0	3.037496
Thrust	β_1	-0.029107
$Thrust^2$	β_2	0.060431
Expander	β_3	1.175450
Gas generator	β_4	1.267294
Pressure feed	β_5	0.831252
Staged combustion	β_6	1.341817

Table 8 summarizes the coefficient values for each cycle which can be substituted in the general equation. This will give us an equation to predict engine dry weight based on a given cycle. By exponentiation of both sides of the equation in Table 7, the following non-linear relationship is established between thrust and weight based on cycle as shown in Table 9.

Table 9: Equations to predict weight for a given thrust based on engine cycle.

Engine Cycle	Logarithmic Equation
Expander Cycle	Log W = (3.037496+ 1.175450) -0.029107*log (Thrust) + 0.060431*$(\log(\text{Thrust}))^{2`}$
Gas Generator Cycle	Log W = (3.037496+ 1.267294) -0.029107*log (Thrust) + 0.060431*$(\log(\text{Thrust}))^2$
Pressure Feed Cycle	Log W = (3.037496+ 0.831252) -0.029107*log (Thrust) + 0.060431*$(\log(\text{Thrust}))^2$
Staged Combustion Cycle	Log W = (3.037496+ 1.341817) -0.029107*log (Thrust) + 0.060431*$(\log(\text{Thrust}))^2$

Since we have a slightly better performing model than the linear model, we can use this to build a predictive model similar to the earlier one and check which one has better performance. The model is setup by creating a training data set and testing data set. The training data set consists of the 80% of the data from our dataset and is used to develop the model. The model is setup in such a way that it chooses the same random data every time which helps us in maintaining a constant dataset. Remaining 20% of the data constitutes the test data set which are solely used for evaluating the performance of the model. Regression model between engine dry weight and thrust is built using the training dataset. This regression model is similar to the model we built in the previous section and can be verified in the similar way. Figure 35 shows a quadratic model fitted to our training data.

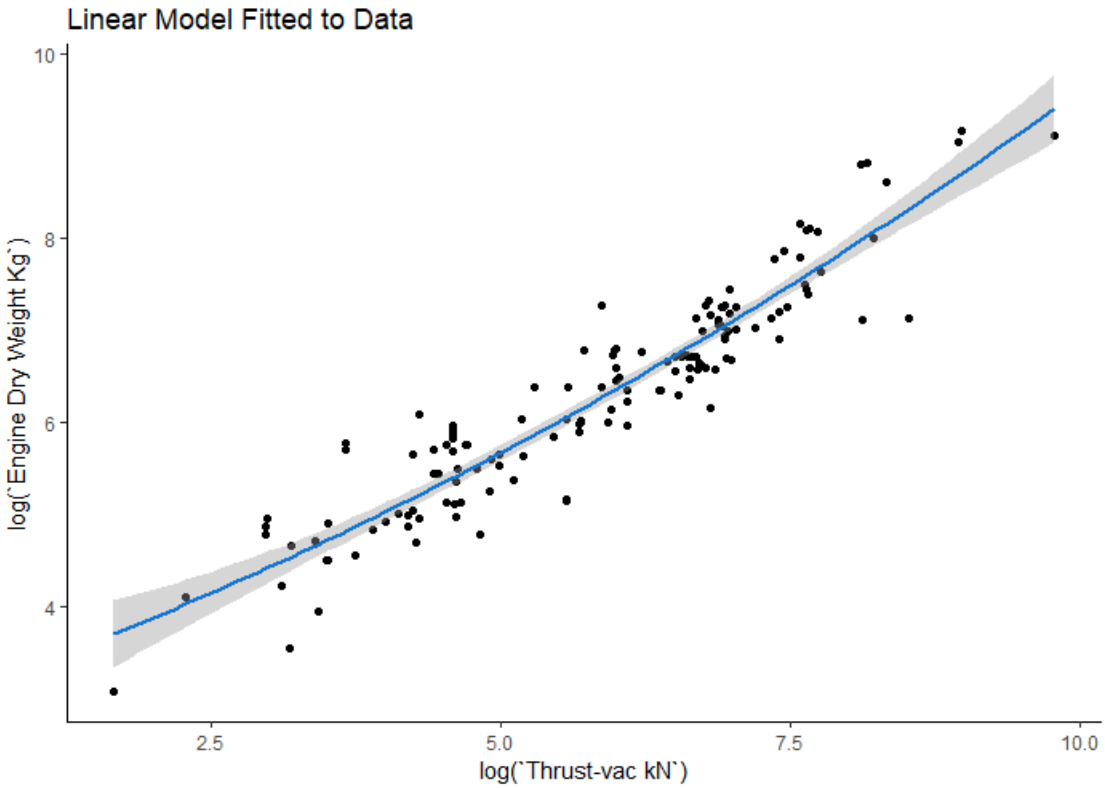

Figure 35: Quadratic model fitted to training data.

The coefficient of determination for this model is $R^2 = 0.8806$, which indicates a strong fit, i.e., 88.06% of the variability in our dataset is explained by the model. Similar to previous sections the residuals of the model can be checked to validate it further. From figure 36 we can clearly see that there are no patterns in our data, and it spread relatively evenly along the horizontal. Normal Q-Q plot shows that the distribution is normal. Histogram of residuals from figure 37 confirms normal distribution as we can see clearly a normal distribution of residuals around zero and the model can be used to proceed further. There are no anomalies in our model, and this can be used for predicting engine dry weight.

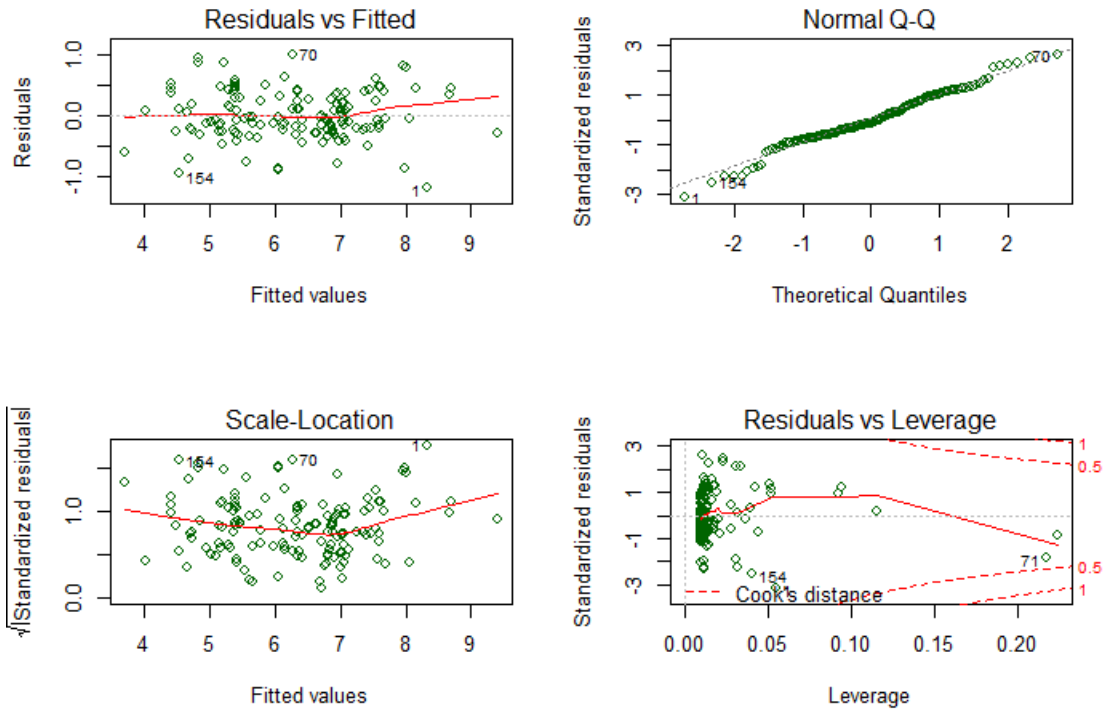

Figure 36: Residual plots of quadratic predictive model.

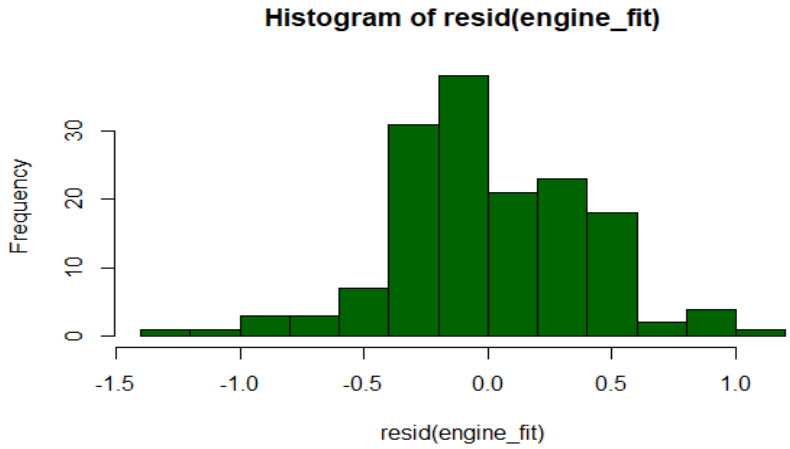

Figure 37: Histogram of residuals.

Now the remaining 20% of data in the testing set is used to make the prediction based on the above model. This will reveal the accuracy of the model we built. A linear fit to the predictive model produced a coefficient of determination R^2 of 0.9301 which implies the model can explain 93.01% of variance in the data and its prediction is quite accurate. Since our model is log based the predicted values are log based as well. This value can be exponentiated to find out the actual value of engine dry weight. Predicted value and the actual values is plotted as shown in figure 38 to check for linear spread of data. As we can see the data is spread linearly.

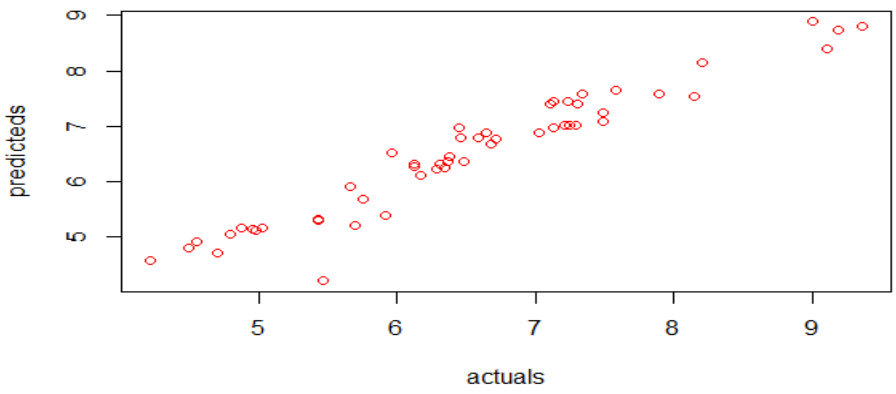

Figure 38: Actual vs Predicted value

There are couple of other methods to estimate the accuracy and error percentage of our predictive model. Min/Max accuracy will find out the accuracy of each row. It takes for each row the ratio of minimum and maximum of the prediction result. For a perfect model this measure is 1. Taking the mean of this measure over the entire model gives us the accuracy rate of each row which can be considered the accuracy rate of the model. Our predictive model has a min/max accuracy of 0.9616 or our model prediction is 96.16% accurate. Mean absolute percentage error is the average of absolute percentage errors which is the measure of the prediction accuracy of a model. MAPE value for our model is 0.03946 or 3.95% which indicates our model has an error percentage of 3.95% in its prediction of engine dry weight.

When compared with predictive model of linear regression the quadratic model fits our data slightly better and the predictions are also slightly better. This argument can be verified through k fold cross validation. A 10-fold cross validation for a simple quadratic model had a R-squared of 0.8958, RMSE of 0.3759 and MAE of 0.293. The quadratic model based on cycles had a R-squared of 0.90775, RMSE of 0.3676 and MAE of 0.289. These results show that the quadratic model based on cycles has a slightly better prediction capability.

Chapter IV

Physical interpretation of the model through dimensional analysis

4.1 Overview

With the advent of very large liquid propellant rockets, it has become necessary, if possible, to derive a rational scaling theory for design of liquid propellant rocket engines including various components that goes into it. This could enable a relatively simple and economical initial tests to be carried out on small scaled models using scaled parameters of propellant mass flows, pressure etc., and from these tests predict operating and design data for the full-scale rocket. Due to the complexity involved the similarity criteria should extend over several non-dimensional parameters, but it is still possible to evolve relatively simple rules for correlating the design and performance of the model and large-scale motors [64]. This chapter attempts to discuss and establish such practical feasibility of such scaling rules.

Dimensional analysis can be used to reduce such a complex physical problem to a simple form prior to obtaining a quantitative answer. The principal use of dimensional analysis is to deduce from a study of the dimensions of the variables in any physical system certain limitations on the form of any possible relationship between those variables. This method is of great generality and mathematical simplicity. At the heart of dimensional analysis is the concept of similarity. In physical terms, similarity refers to some equivalence between two things or phenomena that are different [65]. Our model proved a relationship between weight and thrust and this can be proved mathematically by dimensional analysis.

On traditional liquid-fueled launch vehicles, the engines themselves tend to weigh about twice as much as the payload being delivered to orbit. At launch, they are required to produce a thrust slightly larger than the total weight of the vehicle. If they could produce this same thrust while weighing much less, this weight savings could be used to increase the mass of the payload. There are two ways that the thrust-to-weight ratio can be increased for a given propellant combination.

1. Higher combustion chamber pressure will lead to a smaller engine for a given thrust level.
2. By making the engine smaller at constant chamber pressure, the thrust-to-weight ratio will increase, everything else being equal. This is because the thrust produced is proportional to the throat area, while the weight of the engine is proportional to its volume. For perfect scaling, the ratio of the throat area to the overall volume will increase as the rocket is made smaller.

4.2 Scaling Laws

The scaling of parameters of interest can reveal the underlying physics behind the statistical analysis of a system's descriptors. The data analysis has shown compellingly that broadly speaking there is a power law relationship between the weight (mass) of a liquid rocket engine core and the thrust produced. Specifically, the relationship is essentially:

$$W = KT^{0.7} \quad (4.1)$$

meaning that thrust scales to a higher degree with length scale than weight.

Weight scales with volume which scales as length scale (l) cubed. Thrust is more nuanced. One way to represent thrust is using the thrust coefficient.

$$T = C_F P_o A^* \qquad (4.2)$$

In Equation 4.2, C_F is thrust coefficient, P_o is Chamber stagnation Pressure and A^* is the nozzle throat area. For solid rocket motors the gas is generated by burning propellant at high pressure in a static, confined chamber and it can be shown that with conventional burn rate models, chamber pressure is independent of length scale and thrust is left to scale with throat area (length scale squared). Many additional conclusions follow from some simple similitude arguments for solid motors; however, for liquid engines, the high pressure, high enthalpy gas must be generated using turbomachinery and the turbomachinery is in part the weight that is being modeled using statistically defensible analysis with a simple basis function. For this arrangement in which a gas is generated by turbomachinery, the pressure must be maintained by the function of the turbomachinery. The amount of power produced by the turbomachinery is linearly proportional to the pressure, in fact. To explore this idea, consider a gas being driven through a nozzle by a piston/cylinder arrangement as shown in Figure 39.

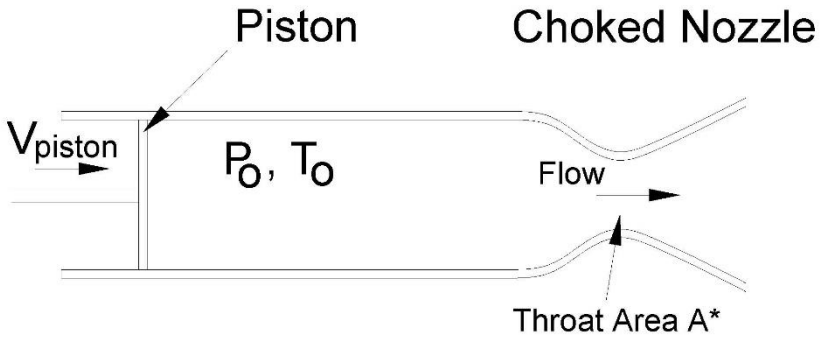

Figure 39: Piston/Cylinder arrangement.

Consider the equilibrium case in which a given piston speed correlates to an equilibrium pressure and nozzle flow rate. If the piston speed increases, the chamber pressure and thus the nozzle mass flow will increase (from isentropic nozzle flow theory). The power would then increase as well.

The case of interest in the similitude analysis is the condition in which the pressure and throat area are specified for a prescribed (known) thrust. In that case the power required to drive the piston and thus supply the nozzle with hot gas at pressure P_o is equal to the piston area multiplied by the linear speed of the piston. Dimensionally this is l^3/time. Therefore, the size of hardware required to drive the nozzle with a prescribed chamber pressure scales with length scale cubed. This consistent for example with the idea that the power of a piston engine is related to the volumetric displacement of the engine for a given design. Since the thrust demands pressure with hardware associated with length scale cubed multiplied by a characteristic (throat) area of length scale squared, the length scale required for thrust is of degree 5, or

$$T = P_o \text{ (order } l^3\text{) x } A^* \text{ (order } l^2\text{)} \quad \text{or T is order } l^5$$

This implies that weight (order l^3) should equal thrust (order l^5) raised to the 3/5 or 0.6 power. The statistical analysis arrived at weight equals thrust raised to the 0.7 power, very consistent with the foregoing dimensional analysis given the assumptions involved including the fact that the turbopump hardware was lumped with the nozzle and other hardware.

Being able to understand and use the basic scaling laws is a very powerful tool. Dimensional analysis of other parameters showed that mass flow rate is proportional to area and as the area increases mass flow rate increases as $L^{1.5}$. Power required by the turbopump is proportional to cube of mass flow rate which means that as the power required increases, the mass of the turbopump increases by a factor of 3 (Power = M^3).

Also, the weight of the pump casing is proportional to the radii of pump impellers. Impeller weight is proportional to the square of its radii. The turbine weight depends on the rotational speed and its inversely proportional [66]. The overall weight for a given propellant mass flow mainly depends on the rotational speed which is fixed by conditions in the pump normally dependent on

the oxidant pump. The higher the oxidant density results in higher rotational speed and hence results in smaller dimensions and weight. This can be illustrated by comparing turbo pumps required for the same rocket engine performance, but using different oxidants entailing different fuel/oxidant mixture ratios [66]. If data can be compiled for all these different relations, it can be visualized, and a model can be built to establish a statistically defensible relationship which can make the process of designing a liquid propellant rocket engine much simpler and economical.

4.3 Practicality of the Scaling Laws

As is often the case, reality and practicality get in the way of theory. According to our argument above we can use multiple engines instead of a single engine approach for the core stage. This approach was used to varying degrees in both the US and Soviet moon programs. The first stage of the Saturn V was powered by five F-1 engines, saving about half the weight of an equivalent single engine according to the above argument. The Soviet launcher was to be powered by about 25 engines [65]. By the arguments above, one would have expected that together they weighed about a fifth of an equivalent single engine. The rocket never had a successful flight as there were a number of single engine failures that led to failure of the launch system. A system with a large number of engines has the capability to provide redundancy in that the loss of thrust from one could have only a small effect on total thrust level. However, if the failure of one engine cannot be contained, additional engines will multiply the number of single point failure modes for the launch system, leading to significantly reduced overall system reliability [65].

Other practical issues arise as well. One must justify the additional complexity required in the pluming and control of many versus few engines. Additionally, the traditional view is that there

is a minimum chamber residence time required for complete combustion in rocket engines, which does not scale with size. This means that one cannot perform an exact scaling of the engines without sacrificing efficiency, something launch vehicle designers are quite loathed to do.

Cost is another concern. Using traditional manufacturing methods, the cost of producing one half-size engines is probably not much less than the cost of producing a full-sized engine, as in a perfect scaling each of the pieces would have to be reproduced at half-scale. The cost of a smaller engine might even exceed that of a larger one as it becomes harder to reproduce the detail of the original pieces at smaller and smaller scales. Eventually, limits in fabrication technology would prevent one form successfully making the smaller engine. In any case, the cost per unit thrust of an engine would certainly increase [65].

It is quite clear that the reduction in scale of rocket engines is not a so-called ‘silver-bullet’ automatically leading to better system performance. As is usually the case, a high-level system trade-off is required in choosing the appropriate number and size of engines for a given propulsion system. The new concept of rockets which are micro-fabricated from silicon-carbide appear provide substantial benefits to the scaling laws [65]. Also, advancements in manufacturing techniques like 3D printing, emergence of better class of materials with maximum utilization, costs could be driven down. It is when we will see the full benefits of scaling laws in terms of cost savings, reducing the development costs significantly.

CHAPTER V

CONCLUSION

Relationship between engine dry weight and thrust which was revealed through the visualization of our data has been explored further through regression models with satisfactory results. All four models are a good fit to our data and each one is slightly better than the other. All the models can satisfactorily predict engine dry weight given a thrust value. Especially the models based on cycle have a slightly better prediction accuracy than the regression model applied to the data as a whole. We can compare the two regression models based on cycles and look at their prediction interval. Figure 40-41 shows the prediction interval of model based on cycles.

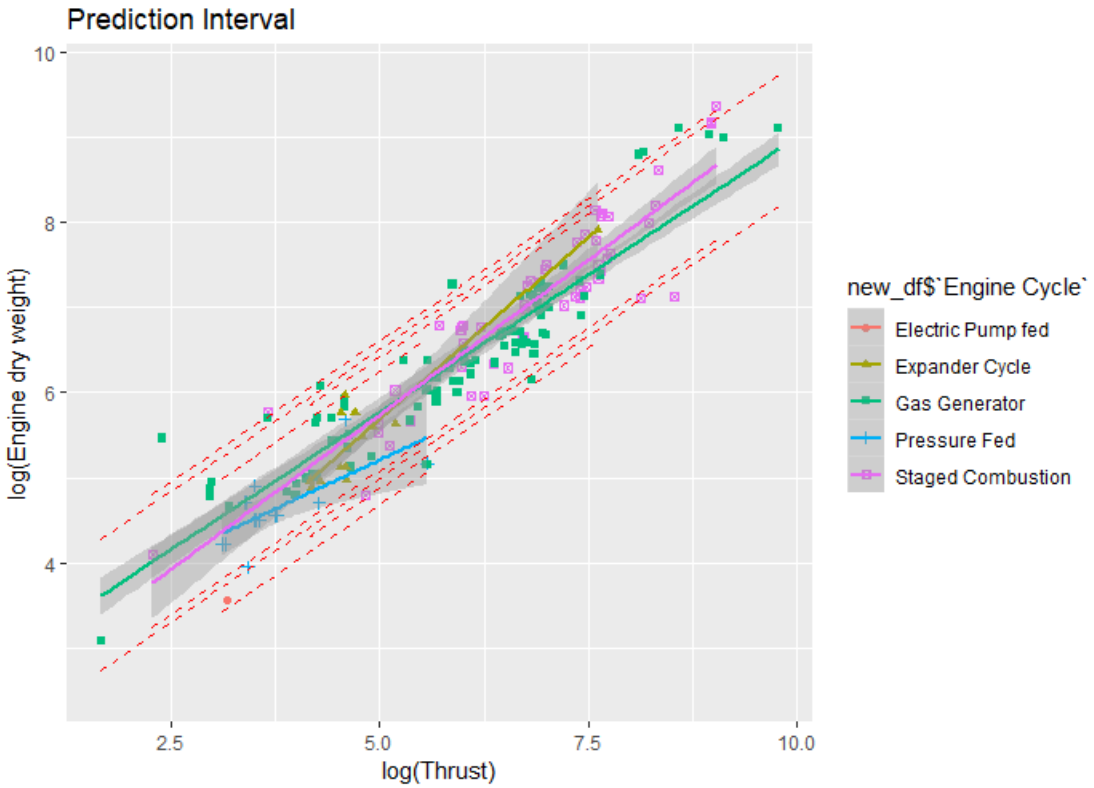

Figure 40: Prediction interval for linear model.

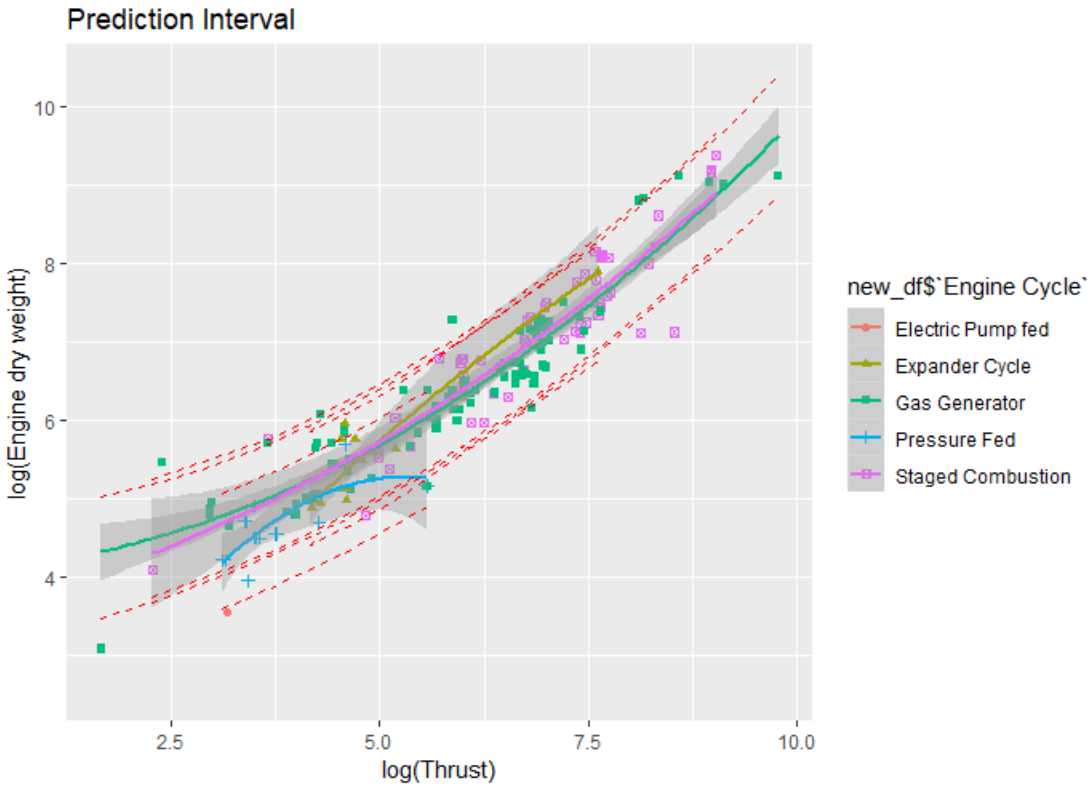

Figure 41: Prediction interval for quadratic model.

Both the models do a good job of prediction and the quadratic model is slightly better than the linear model. Still, both can be used to predict engine dry weight and it is only a matter of preference in choosing between both. Since the model is log based there tends to be slight variations in range of the predicted values when they are exponentiated to the raw scale. This can be attributed to the variety of engine data that was collected from all over the world. This tends to have some effects in terms that each of these engines have their own design process, material selection, manufacturing approaches depending on their country of origin and the year in which they were developed.

Engines developed in the 60's tend to have used traditional manufacturing methods and materials than the one's developed in the 2000's. There has been immense advancement in manufacturing processes and available materials. Advanced engines of today built entirely using 3D printing is most likely to weigh much less than the same class of engine built using traditional manufacturing methods. Despite these differences our model does a good job of predicting the engine dry weight as verified through dimensional analysis. As discussed in the previous chapter, the relationship between other parameters can be explored further provided the availability of enough data. If a statistically defensible relationship can be established between those parameters, scaling laws can be robustly applied to the design of liquid propellant rocket engines which could very well save millions of dollars during the development phase of a new engine.

References

1. Mark Carpenter and Roy Hartfield, “Similitude for Dry Liquid Rocket Engines.” AIAA Paper 2018-4548. Joint Propulsion Conference, Cincinnati, Ohio. 2018.

2. Barrere, M., Jaumotte, A., Veubeke, B., and Vandenkerckhove, J., Rocket Propulsion, Elsevier Publishing Company, Amsterdam, 1960.

3. George P. Sutton, Oscar Biblarz, Rocket Propulsion Elements, seventh edition, John Wiley & Sons, 2001.

4.Nancy Hall, “Rocket Thrust Equation”, NASA Glenn Research Center, https://www.grc.nasa.gov/www/k-12/airplane/rockth.html, retrieved 02 February 2019.

5.Qualitative Reasoning Group, “Specific Impulse”, Northwestern.edu, http://www.qrg.northwestern.edu/projects/vss/docs/propulsion/3-what-is-specific-impulse.html, retrieved 18 February 2019.

6. Benson, Tom. “Specific Impulse”, NASA Glenn Research Center, https://www.grc.nasa.gov/WWW/K-12/airplane/specimp.html, retrieved 22 February 2019.

7. Khatry, Jivan & Aydogan, Fatih & Ilyas, Muhammad & Houts, Michael. (2018). Design of a passive safety system for a nuclear thermal rocket. Annals of Nuclear Energy. 111. 536-553. 10.1016/j.anucene.2017.09.025.

8. James L. Cannon., Liquid Propulsion: Propellant Feed System Design, NASA NTRS. Encyclopedia of Aerospace Engineering, Volume 2 Propulsion & Power, Wiley Publishers.

9. Michele Raiano, “Power Cycles”, Aerospaceengneering.net, 21 November 2016, http://www.aerospacengineering.net/power-cycles/, retrieved 3 March 2019

10. W. D. Greene, Blogs.nasa.gov, “Inside the J-2X Doghouse: Beyond the Gas Generator Cycle”, retrieved 4 March 2019

11. Sutton, G., History of Liquid Propellant Rocket Engines, AIAA, 2006.

12. AIAA-97-2680: Anisimov V.S./Kuznetsov, T.C.Lacefield/Aerojet, J.Andrews/Kistler: "Evolution of the NK-33 and NK-43 reusable LOX/kerosene engines", AIAA Joint Propulsion Conference July 1997.

13. CADB 93: Information from Chemical Automatics Design Bureau, Voronezh 1993.

14. CADB 96: Rachuk V.: "Best Rocket Engines from Voronezh", Aerospace Journal, Moscow, Nov-Dec. 1996.

15. CADB+AJ 95: Gontcharov, Orlov, Rachuk, Rudis, Shostak, McIllwain, Starke, Hulka: "Tripropellant Liquid Rocket Engine Technology Using a Fuel-Rich Closed Power Cycle", ONERA, June 1995.

16. "Energia 46-96": "RKK Energia 1946-96", Korolyov 1996.

17. Eurockot 98: "ROCKOT Users Guide", issue 2 rev. 0, Eurockot Launch Services, Bremen 1998.

18. Energia 94: S P Korolev Space Corporation Energia, English-Russian book, 1994.

19. Glushko 69: Glushko V.P.: "Albom Konstruktsiy ZhRD" (Album of Liquid Rocket Engine Developments), Vol. 1 1968, Vol. 3 & 4 1969.

20. Glushko 85: Glushko V.P. (ed.): "Kosmonavtika Entsiklopedia", Moscow 1985.

21. Gubanov 91: Gubanov B.I.: "USSR Main Engines for Heavy-Lift Launch Vehicles: Status and Direction" AIAA-91-2510, AIAA-Joint Propulsion Conference, Sacramento June 1991.

22. IAF-97-S.1.03: Klepikov, Katorgin, Chvanov: "The New Generation of Rocket Engines, Operating by Ecologically Safe Propellant ..." NPO Energomash, IAF-Congress Turin, 1997, IAF-97-S.1.03.

23. IAF-97-S.1.04: Shnyakin, Klimov, Shulga: "Uprated Main Liquid Propellant Rocket Engine For CYCLONE LV Third Stage", Yuzhnoe State Design Office, IAF-Congress Turin, 1997, IAF-97-S.1.04.

24. Isakowitz 2: Isakowitz Steven J.: "International Reference Guide to Space Launch Systems", 2nd edition, AIAA, Reston 1995.

25. Johnson 94: Johnson N.L, D.M. Rodvold: "Europe and Asia in Space 1993-1994", USAF Phillips Laboratory, 1995.

26. Kompomash 98-1: Polovnikov S.P., A.S. Karpov: "Projekt 'Vozdushnyy Start'", Vestnik Aviatsii i Ksmonavtiki, Moscow, 1-2/98.

27. Fanciullo, Lacefield: "High Performance Russian D-57 LH2/LOX Rocket Engine", AIAA-94-3398, AIAA Joint Prop. Conf., June 1994.

28. MAKS 95: Catalogue and datasheets at Moscow Aerospace Exhibition, Moscow-Shukovski, 1995.

29. Pavutn. 96: Pavutniskiy Yu.M., V.A. Mazarchenko, M.V. Shilenkov, A.B. Gerasimov: "Otechestvennye Rakety-Nositeli", St.Peterburg (State Marine-Technol. Univ.), 1996.

30. "Raketi nad Morem": Shirokorad A.: "Rakety nad Morem", 2nd edition, in: 'Tekhnika I Vooruzhenie', Moscow 11-12, 1997.

31. Russian Arms Cat.: Russian Arms Catalogue, Vol. 6 & 4, Military Parade, Moscow.

32. Starsem 97: Starsem: "Soyuz Launcher User manual", issue 2 rev. 0, Starsem Paris 1997.

33. Starsem 99-2: Starsem: "Launch Kit Flight 02", Starsem Paris 1999 (http://www.starsem.com/newsst_kit.html).

34. Varfolomeyev: Varfolomyev T.: "Soviet Rocketry that Conquered Space - Parts 1-8", Spaceflight, London 1995-98.

35. Wade: Mark Wade: "Encyclopedia Astronautica", internet http://solar.rtd.utk.edu/~mwade/engines/engindex.htm, retrieved 17 December 2018.

36. Yuzhnoe 96: Shnyakin V.N.: "Shidkostnye Raketye Dvigateli - Opisanie i Osnovnye Tekhnicheskie Dannye", GKB Yuzhnoe "Yangel", Dnepropetrovsk 1996.

37. Energomash 93: NPO Energomash exhibit at Moscow Airshow MAKS 93, Moscow, 1993.

38. Glushko 87: Glushko V.P.: "Razvitie Raketostroeniya i Kosmonavtiki v SSSR", Moscow 1987.

39. “Aestus Rocket Engine”. Airbus Defence and Space. en.wikipedia.org, retrieved 23 December 2018

40. “GSLV Launnch Vehicle information” spaceflight101.com, retrieved 27 December 2018

41. Alternate Propulsion Subsystem Concepts NAS8-39210 DCN 1-PP-02147. April, 1993.

42. “J-2X engine”, Pratt & Whitney Rocketdyne, retrieved 26 November 2018

43. “Falcon 9 Space Launch Report”. SpaceLaunnchReport, 2015, retrieved 4 January 2019.

44. “Merlin 1D”. SpaceX report, 2015, retrieved 5 January 2019.

45. “SpaceX Falcon 9 Product Page”. SpaceX.com, 2014, 5 January 2019.

46. “Vulcain”, Airbus defense and space, retrieved 8 January 2019.

47. “Chinese YF-100”. SPACEPAC. spacepac.org, retrieved 18 November 2018.

48. Michael Galarnyk., “Understanding Boxplots”. towardsdatascience.com, retrieved 16 March 2019.

49. Robert McGill, John W. Tukey and Wayne A. Larsen., “Variations of Box Plots”. The American Statistician Vol. 32, No 1, Feb., 1978.

50. Frigge, Michael, et al. “Some Implementations of the Boxplot.” *The American Statistician*, vol. 43, no. 1, 1989, pp. 50–54. *JSTOR*, www.jstor.org/stable/2685173.

51. Alboukadel Kassambara, “Correlation Test Between two variables in R”, www.sthda.com, retrieved 27 March 2019.

52. Alvin C. Rencher and G. Bruce Schaalje. “Linear Models in Statistics”, second edition, John Wiley & Sons, 2008.

53.Selva Prabhakaran, “Linear Regression”, r-statistics.co, retrieved 13 April 2019.

54. R. Dennis Cook and Sanford Weisberg. “Residuals and Influence in Regression”, first edition, Chapman and Hall, 1982.

55. Brady Ingrid, “Residual Analysis”, rpubs.com, retrieved 18 May 2019.

56. Michelle Lacey, “Multiple Linear Regression”, www.stat.yale.edu, retrieved 23 May 2019.

57. David Salgado, “Data Science for Developers: Build your First Predictive Model with R”, medium.com/@davidsb/datascience-for-developers-build-your-first-predictive-model-with-r, retrieved 16 June 2019.

58. Rose Martin, “Using Linear Regression for Predictive Modeling in R”, www.dataquest.io, retrieved 24 June 2019.

59. Sergio Venturini, “Cross-Validation for Predictive Analytics Using R”, www.milanor.net, retrieved 8 July 2019.

60. Jake Drew, “How to split a data set to do 10-fold cross validation”, Stats.stackexchange.com, retrieved 10 July 2019

61. Peter Flom, “R using linear and quadratic term in regression model”, stats.stackexchange.com/questions/262269/r-using-linear-and-quadratic-term-in-regression-model, retrieved 10 July 2019

62. “How to plot quadratic regression in R”, stackoverflow.com/questions/26959527/how-to-plot-quadratic-regression-in-r, retrieved 11 July 2019

63. David Lillis, “Fitting a Quadratic Model”, www.theanalysisfactor.com, retrieved 12 July 2019

64. Sethna, C. (2014). Scaling theory for liquid propellant rocket thrust chambers. *Defence Science Journal*, *10*(2), 115-123. https://doi.org/10.14429/dsj.10.7659

65. Adam London, Daniel Kirk, “Comments on Rocket Scaling”, retrieved 14 July 2019

66. D.J. Saunders, “A method of calculating the weight and dimensions of a turbo pump for rocket propellants”. Technical note R.P.D. 22.

APPENDIX – A

	Engine	Engine Cycle	Engine Dry Weight Kg	Thrust-vac kN	Isp-vac [sec]	Thrust/Weight Ratio
1	AJ-26-58/-59	Staged Combustion	1240	5056.8	331.3	415.7048436
2	AJ-26-60	Staged Combustion	1400	1769	348.3	128.804427
3	AJ-26-62	Staged Combustion	1222	3371.2	334	281.2187704
4	LE-7	Staged Combustion	1714	1078	446	64.11194254
5	LE-7A	Staged Combustion	1800	1098	438	62.1814475
6	NK-15	Staged Combustion	1247	1544	318	126.215251
7	NK-15V	Staged Combustion	1345	1648	325	124.901
8	NK-31	Staged Combustion	722	402	353	56.75705439
9	NK-33	Staged Combustion	1222	1638	331	136.6386883

10	NK-39	Staged Combustion	631	402	352	64.94230313
11	NK-43	Staged Combustion	1396	1755	346	128.1512053
12	Plug-Nozzle SSME	Staged Combustion	2973	3728.7	485	127.8478786
13	RD-0120	Staged Combustion	3450	1961	455	57.94146759
14	RD-0120-CH	Staged Combustion	2370	1576	363	67.78582089
15	RD-0120K	Staged Combustion	1433	873	336	62.10106468
16	RD-0120M	Staged Combustion	3450	1961	455	57.94146759
17	RD-0120M-Methan	Staged Combustion	2600	1720	372	67.43511331
18	RD-0126	Staged Combustion	320	39.2	476	12.4872579
19	RD-0134	Staged Combustion	1800	2038	358	115.4151093
20	RD-0139	Staged Combustion	1544	2038	341	134.5512932

21	RD-0140	Staged Combustion	1689	2086	349	125.897077
22	RD-0141	Staged Combustion	1973	2251	353	116.2999164
23	RD-0142	Staged Combustion	2058	2353	369	116.548731
24	RD-0144	Staged Combustion	250	147	374	59.93883792
25	RD-0145	Staged Combustion	282	147	374	53.13726766
26	RD-0210-HC	Staged Combustion	566	582.1	327	104.8364149
27	RD-0234-Kerosene	Staged Combustion	390	516	331	134.8702266
28	RD-0234-Methan	Staged Combustion	390	442	343	115.5283724
29	RD-0242-Kerosene	Staged Combustion	120	125	312	106.1841658
30	RD-0244-Kerosene	Staged Combustion	540	690	332	130.2525767
31	RD-0245-Kerosene	Staged Combustion	290	214	320	75.22232767

32	RD-0256-Kerosene	Staged Combustion	770	820	344	108.5560719
33	RD-0256-Methan	Staged Combustion	770	836	353	110.6742391
34	RD-100	Staged Combustion	885	304	237	35.01557848
35	RD-101	Staged Combustion	888	404	237	46.37665188
36	RD-103	Staged Combustion	870	500	243	58.58436735
37	RD-103M	Staged Combustion	867	500.1	248	58.79883884
38	RD-120	Staged Combustion	1125	833	350	75.47853664
39	RD-120K	Staged Combustion	1433	873	336	62.10106468
40	RD-120M	Staged Combustion	1080	850.4	331	80.26579077
41	RD-169	Staged Combustion	215	167	351	79.17881611
42	RD-170	Staged Combustion	9750	7903	337	82.62631015

43	RD-171	Staged Combustion	9500	7903	337	84.80068673
44	RD-172	Staged Combustion	11703	8354	337	72.76595919
45	RD-180	Staged Combustion	5480	4152	339	77.23386683
46	RD-182	Staged Combustion	1500	902	353	61.29799524
47	RD-183	Staged Combustion	60	9.8	360	16.6496772
48	RD-185	Staged Combustion	415	179	378	43.96792061
49	RD-190	Staged Combustion	1470	1000	351	69.34476135
50	RD-191	Staged Combustion	3230	2079	337	65.61195217
51	RD-192	Staged Combustion	3300	2138	356	66.0426899
52	RD-57	Staged Combustion	840	392	457	47.57050629
53	RD-57A-1	Staged Combustion	550	395	460	73.20915578

54	RD-57M	Staged Combustion	874	397	461	46.30309986
55	RD-701	Staged Combustion	3670	4003	460	111.1861055
56	RD-704	Staged Combustion	2422	1966	407	82.7447346
57	SSME	Staged Combustion	3177	2278	453	73.09160483
58	SSME Plus	Staged Combustion	2973	3728.7	467	127.8478786
59	YF-100	Staged Combustion	1124	1339.48	335	121.4789179
60	Aestus	Pressure Fed	111	29.4	321.3	26.99947654
61	Aestus+	Pressure Fed	111	30	323.8	27.55048627
62	AJ-10-118	Pressure Fed	90	33.1	263	37.49008948
63	AJ-10-118D	Pressure Fed	90	33.7	272.5	38.16966814
64	AJ-10-118E	Pressure Fed	90	35.2	278	39.86861479
65	AJ-10-118F	Pressure Fed	95	42.3	315	45.38870111
66	AJ-10-118K	Pressure Fed	95	43.4	320.5	46.56902194
67	AJ-10-137	Pressure Fed	294	97.9	301.4	33.94426068
68	AJ-10-138	Pressure Fed	110	71.7	311	66.4442591

69	AJ-10-190	Pressure Fed	135	33.4	294.3	25.21991921
70	Astris 1	Pressure Fed	68	22.6	300	33.87899502
71	Astris 2	Pressure Fed	68	23.3	310	34.92834443
72	Kestrel	Pressure Fed	52	30.7	320	60.18191798
73	Vexin A (2)	Pressure Fed	175	262	281	152.6139508
74	17D11	Gas Generator	230	86.3	362	38.24845987
75	17D12	Gas Generator	230	86.3	362	38.24845987
76	A-6	Gas Generator	658	414.3	265	64.18300289
77	A-7	Gas Generator	658	416.2	265	64.47734927
78	Aestus-2	Gas Generator	138	55	337	40.62698518
79	CE-20	Gas Generator	588	200	443	34.67238068
80	CE-7.5	Gas Generator	435	73.5	454	17.223804
81	F-1	Gas Generator	8391	7740.5	304	94.03429795
82	F-1A	Gas Generator	8098	9189.6	310	115.6777488

83	F-1B	Gas Generator	9015	17633	299	199.3845347
84	Gamma 2	Gas Generator	173	262	257	154.3782739
85	Gamma 8	Gas Generator	342	234.8	265	69.98467967
86	H-1	Gas Generator	635	947.7	289	152.1346529
87	H-1b	Gas Generator	988	1030.2	296	106.2907799
88	HM-10	Gas Generator	145	61.8	443	43.44616682
89	HM7-A	Gas Generator	149	61.7	443	42.21141282
90	HM7-B	Gas Generator	155	70	447	46.03597383
91	J-2	Gas Generator	1438	1033.1	421	73.23428876
92	J-2S	Gas Generator	1400	1138.5	436	82.89646134
93	J-2-SL	Gas Generator	1360	996.7	390	74.70618217

94	LE-5	Gas Generator	245	103	450	42.85506251
95	LH2-80k	Gas Generator	1438	355.7	425	25.21482578
96	LR-101-11	Gas Generator	21.8	5.3	246	24.7827998
97	LR-105-5	Gas Generator	460	386.4	316	85.62691131
98	LR-105-7	Gas Generator	460	386.4	316	85.62691131
99	LR-79-7	Gas Generator	643	758.7	282	120.2790817
100	LR-87 LH2	Gas Generator	700	667	350	97.13120722
101	LR-87-3	Gas Generator	839	733.9	290	89.16736224
102	LR-89-5	Gas Generator	720	822.5	290	116.4486352
103	LR-89-7	Gas Generator	711.5	948	294	135.8202187
104	LR91-11	Gas Generator	590	467	316	80.68556817

105	LR91-3	Gas Generator	590	355.9	308	61.49035056
106	LR91-5	Gas Generator	500	444.8	315	90.68297655
107	LR91-7	Gas Generator	565	444.8	316	80.25042173
108	M-1	Gas Generator	9068	5335.9	428	59.98285915
109	MA-5A	Gas Generator	1610	2100	296	132.9610424
110	MB-3 Press Mod	Gas Generator	643	755.1	285	119.7083625
111	MB-3-1	Gas Generator	643	760.6	285	120.5802946
112	MB-3-3	Gas Generator	723	866.7	290	122.1972667
113	MB-60	Gas Generator	591	266.7	467	46.00092105
114	Merlin 1A	Gas Generator	402	378.04	310	95.86116309
115	Merlin 1C	Gas Generator	582	411.4	342	72.05635599

116	Merlin 1D	Gas Generator	470	914	311	198.2345414
117	RD-0105	Gas Generator	125	49.4	316	40.28542304
118	RD-0107-11D511	Gas Generator	410	297	326	73.84202282
119	RD-0109	Gas Generator	121	54.52	324	45.93053134
120	RD-0110	Gas Generator	405	297.9	326	74.98017896
121	RD-0124	Gas Generator	480	294.3	359	62.5
122	RD-0124M	Gas Generator	360	294.3	348	83.33333333
123	RD-0124M1	Gas Generator	393	294.3	359	76.33587786
124	RD-0126A	Gas Generator	340	98	476	29.38178329
125	RD-0126E	Gas Generator	300	39.2	472	13.31974176
126	RD-0128	Gas Generator	370	98	474	26.99947654

127	RD-0131	Gas Generator	350	98	467	28.54230377
128	RD-0132	Gas Generator	370	98	469	26.99947654
129	RD-0210-Kerosene	Gas Generator	570	592	342	105.871202
130	RD-0245-HC	Gas Generator	290	214	320	75.22232767
131	RD-105	Gas Generator	782	627.6	302	81.81014727
132	RD-106	Gas Generator	802	645.3	310	82.01972134
133	RD-107-8D728	Gas Generator	1145	996	314	88.67166112
134	RD-107-8D74	Gas Generator	1155	971	306	85.69751689
135	RD-107-8D74K	Gas Generator	1145	996	313	88.67166112
136	RD-107-8D74PS	Gas Generator	1155	971	306	85.69751689
137	RD-107-8D75	Gas Generator	1250	941	315	76.73802243

138	RD-107-8D76	Gas Generator	1155	971	310	85.69751689
139	RD-108 - 11D512P	Gas Generator	1400	1011	319	73.61293141
140	RD-108 - 8D727	Gas Generator	1230	977	316	80.96931122
141	RD-108 - 8D75K	Gas Generator	1252	941	315	76.61543773
142	RD-108 - 8D77	Gas Generator	1250	804	315	65.56574924
143	RD-108 - 11D512	Gas Generator	1400	997	315	72.59356342
144	RD-108 - 8D75	Gas Generator	1278	912	308	72.74363134
145	RD-108-11D512	Gas Generator	1400	997	315	72.59356342
146	RD-108-8D727	Gas Generator	1230	977	316	80.96931122
147	RD-109	Gas Generator	210	101.6	334	49.31799427
148	RD-111	Gas Generator	1492	1628	317	111.2286254

149	RD-112	Gas Generator	790	1089	344	140.5179422
150	RD-113	Gas Generator	1100	1138	360	105.4582522
151	RD-114	Gas Generator	990	1653	341	170.2035647
152	RD-115	Gas Generator	1250	1726	357	140.7543323
153	RD-119	Gas Generator	168	105.5	352	64.01388282
154	RD-134	Gas Generator	540	343	357	64.74874467
155	RD-160	Gas Generator	129	19.6	381	15.48807181
156	RD-161 (1)	Gas Generator	119	19.6	360	16.78959045
157	RD-161 (2)	Gas Generator	141	19.9	365	14.38682485
158	RD-161P	Gas Generator	105	24.5	319	23.78525314
159	RD-167	Gas Generator	570	353	379	63.1292809

160	RD-56	Gas Generator	282	69.6	462	25.15886959
161	RD-58	Gas Generator	300	83.4	349	28.33843017
162	RD-58M	Gas Generator	230	83.4	353	36.96316979
163	RD-58MF	Gas Generator	230	83.4	353	36.96316979
164	RD-58S	Gas Generator	230	86.3	361	38.24845987
165	RD-58Z	Gas Generator	300	71	361	24.12504247
166	RS-27	Gas Generator	1027	1023	295	101.5397717
167	RS-27A	Gas Generator	1091	1054.2	302	98.49841769
168	RS-27C	Gas Generator	1091	1054.2	302	98.49841769
169	RS-56-OBA	Gas Generator	805	1046.8	299	132.5558278
170	RS-56-OSA	Gas Generator	460	386.4	316	85.62691131

171	RS-68	Gas Generator	6597	3312	420	51.1770015
172	RS-68A	Gas Generator	6747	3503.5	414	52.93249977
173	RZ.2	Gas Generator	750	836.3	282	113.6663269
174	S1.5400	Gas Generator	153	66.69	340	44.43245188
175	S1.5400A	Gas Generator	148	67.3	342	46.35369314
176	S-3	Gas Generator	725	758.7	282	106.6751028
177	Viking 4	Gas Generator	826	713	290	87.99145014
178	Viking 4B	Gas Generator	826	784.8	291	96.85230024
179	Viking 4B+	Gas Generator	826	807.8	293	99.69073412
180	Viking 5	Gas Generator	826	667.5	268	82.37628748
181	Viking 5B	Gas Generator	826	720	271	88.85532132

182	Viking 5C	Gas Generator	826	760.5	278	93.85343315
183	Viking 6	Gas Generator	826	749	274	92.43421621
184	Vulcain	Gas Generator	1300	1075	431	84.29389163
185	Vulcain 2	Gas Generator	1800	1350	434	76.45259939
186	X-405	Gas Generator	191	134.8	270	71.94283
187	XLR-105-5	Gas Generator	460	363.2	309	80.48575101
188	XLR-89-1	Gas Generator	725	758.7	282	106.6751028
189	XLR-89-5	Gas Generator	643	758.7	282	120.2790817
190	XLR-99	Gas Generator	414.9659864	262.4	276	64.45881586
191	YF-20B	Gas Generator	712.5	816.3	289	116.7873813
192	YF-73	Gas Generator	236	11	425	4.751291487

193	LE-5A	Expander Cycle	242	121.5	452	51.17901281
194	LE-5B	Expander Cycle	269	137	447	51.91576761
195	RD-0133	Expander Cycle	390	98	467	25.614888
196	RL-10	Expander Cycle	131	66.7	410	51.9021718
197	RL-10A-1	Expander Cycle	131	66.7	425	51.9021718
198	RL-10A-3	Expander Cycle	131	65.6	444	51.04621394
199	RL-10A-3A	Expander Cycle	141	73.4	444	53.06497206
200	RL-10A-4	Expander Cycle	168	92.5	449	56.12591622
201	RL-10A-4-1	Expander Cycle	167	99.1	451	60.49063952
202	RL-10A-4-2	Expander Cycle	167	99.1	451	60.49063952
203	RL-10A-5	Expander Cycle	143	64.7	373	46.1210553

204	RL-10A-5KA	Expander Cycle	145	100.49	398	70.6457169
205	RL-10B-2	Expander Cycle	317	110	462	35.37239088
206	RL-10B-X	Expander Cycle	317	93.4	470	30.03437553
207	RL-10C	Expander Cycle	317	155.7	450	50.06801146
208	RL-10C-X	Expander Cycle	317	110.8	450	35.62964464
209	SCE-200	Expander Cycle	2700	2030	335	76.64137124
210	VINCI	Expander Cycle	280	180	465	65.53079948
211	Rutherford	Electric Pump fed	35	24	343	69.89951944